Communications Biology

https://doi.org/10.1038/s42003-026-09722-8

Article in Press

CRISPR-Cas9 screening identifies ATOX1-driven cisplatin resistance mechanisms in liver cancer and evaluates targeted inhibitor efficacy

Received: 4 June 2025

Accepted: 6 February 2026

Cite this article as: Hu, C., Tai, H., Zhu, R. *et al.* CRISPR-Cas9 screening identifies ATOX1-driven cisplatin resistance mechanisms in liver cancer and evaluates targeted inhibitor efficacy. *Commun Biol* (2026). https://doi.org/10.1038/s42003-026-09722-8

Chujiao Hu, Huading Tai, Renguang Zhu, Zhengyu Shu, Guanghao Guo, Dan Ma, Shi Zuo, Lei Tang & Zhirui Zeng

CRISPR-Cas9 screening identifies ATOX1-driven cisplatin resistance mechanisms in liver cancer and evaluates targeted inhibitor efficacy

Chujiao Hu[1,2#], Huading Tai[3#], Renguang Zhu[1#], Zhengyu Shu[1], Guanghao Guo[4], Dan Ma[5*], Shi Zuo[2,4*], Lei Tang[1*], Zhirui Zeng[3*]

[1]State Key Laboratory of Discovery and Utilization of Functional Components in Traditional Chinese Medicine, Guizhou Provincial Key Laboratory of Innovation and Manufacturing for Pharmaceuticals, Guizhou Medical University, Guiyang, China;

[2]Key Laboratory for Cancer Prevention and treatment of Guizhou Province, Guizhou Medical University, Guiyang, China;

[3]Transformation Engineering Research Center of Chronic Disease Diagnosis and Treatment, Department of Physiology, School of Basic Medical Sciences, Guizhou Medical University, Guiyang, China;

[4]Department of Hepatobiliary Surgery, The Affiliated Hospital of Guizhou Medical University, Guiyang, China;

[5]Department of hematology, Affiliated hospital of Guizhou Medical University, Guiyang, China

[#] These authors contributed equally

*Corresponding to:

Dan Ma, readying100@163.com;

Shi Zuo, drzuoshi@gmc.edu.cn;

Lei Tang, tlei1974@gmc.edu.cn;

Zhirui Zeng, zengzhirui@gmc.edu.cn

Abstract

Liver cancer treatment with cisplatin is often hindered by drug resistance. This study aimed to identify key genes associated with cisplatin resistance in liver cancer and develop targeted inhibitors. Using genome-wide CRISPR-Cas9 screening, *ATOX1* was identified as a critical gene for cisplatin resistance. ATOX1 was highly expressed in liver cancer tissues and associated with poor prognosis. Knockdown of *ATOX1* in liver cancer cells enhanced cisplatin sensitivity *in vitro* and *in vivo*. Molecular dynamics simulation and virtual screening identified compound 8 as a potent ATOX1 inhibitor with high affinity (Kd = 12.5 μM) and exhibited synergistic effects with cisplatin on liver cancer cell growth. Mechanistically, compound 8 inhibits the activity of ATOX1, leading to intracellular copper accumulation. The elevated copper levels subsequently promote increased DNA methylation at the *NOTCH1* promoter, resulting in suppression of the NOTCH1/HES1 signaling pathway and enhancing the sensitivity of liver cancer cells to cisplatin. In conclusion, ATOX1 is crucial for cisplatin resistance in liver cancer and linked to poor prognosis. Targeting ATOX1 with compound 8 may be a novel therapeutic strategy for overcoming cisplatin resistance.

Keywords: Liver cancer; Cisplatin resistance; ATOX1; CRISPR-Cas9 screening; NOTCH1

Introduction

Liver cancer is the sixth most common malignancy worldwide and a leading cause of cancer-related death [1]. Statistics showed that there are approximately 840,000 new cases and 780,000 deaths from liver cancer globally each year, with Chinese patients accounting for about half of the total cases [2]. Despite recent progress in multiple treatment modalities including surgical resection, local therapies, and systemic treatments, the five-year survival rate of liver cancer patients remains below 20%[3]. This is primarily attributed to late-stage diagnosis, high recurrence rates, and resistance to existing therapeutic approaches [4]. Therefore, exploring the mechanisms of drug resistance in liver cancer and developing novel therapeutic strategies have significant clinical implications [5].

Cisplatin, a classic platinum-based antitumor agent, induces tumor cell apoptosis by forming cross-links with DNA, thereby inhibiting DNA replication and transcription[6]. It is widely used in the treatment of various solid tumors, including liver cancer. However, liver cancer cells often exhibit intrinsic or acquired resistance to cisplatin, severely limiting its clinical efficacy [7]. Currently known mechanisms of cisplatin resistance mainly include decreased drug uptake, increased drug efflux, enhanced DNA damage repair, dysregulated apoptotic pathways, and epigenetic alterations [8]. Among these, metal metabolism-related drug transport systems play a crucial role in cisplatin resistance, though the specific mechanisms remain incompletely elucidated .

Antioxidant Protein 1 (ATOX1) is a copper chaperone protein whose primary function is to transfer intracellular copper ions from the copper transporter CTR1 to ATP7A/B, participating in the maintenance of intracellular copper homeostasis [9, 10]. ATOX1 binds copper ions through its conserved CXXC motif (including Cys12 and Cys15 residues), forming a stable coordination structure [11]. Recent studies have discovered that ATOX1 not only functions in copper metabolism but can also act as a transcription factor directly regulating the expression of various genes involved in cell proliferation, angiogenesis, and tumor invasion [12, 13]. Research indicates that ATOX1 is abnormally expressed in various tumors [14], but its role in liver cancer development and drug resistance has not been thoroughly investigated.

Considering the structural similarity between copper ions and cisplatin molecules and their potentially shared intracellular transport systems, ATOX1 has been implicated in the development of cisplatin resistance [15]. Further, Crystal structure studies have shown that cisplatin can directly bind to the CXXC site of ATOX1, which also serves as the canonical copper-binding site, although the two ligands adopt distinct coordination geometries: cisplatin exhibits square planar coordination, while copper ions typically adopt tetrahedral or dicoordinate geometries [16]. More importantly, cisplatin and copper ions can simultaneously bind to ATOX1, forming stable bimetallic complexes [17]. This binding may cause cisplatin to be sequestered in the cytoplasm, preventing it from reaching its DNA target and thereby reducing its cytotoxicity [18]. Additionally, ATOX1 may transfer bound cisplatin to downstream copper transporters ATP7A/B, further

promoting cisplatin efflux from cells and contributing to the development of resistance [19].

Copper, as an essential trace element in the human body, participates in various physiological processes, including energy production, antioxidant defense, neurotransmission, and cell signaling [20]. Recent research indicates that tumor cells have significantly increased copper requirements, and copper ions can promote tumor angiogenesis, proliferation, invasion, and metastasis [21]. However, copper ions also can influence tumor cell sensitivity to chemotherapeutic agents by regulating multiple signaling pathways [22]. For example, copper can affect the expression and localization of ATP7A/B, thereby regulating intracellular accumulation of cisplatin; it can also indirectly influence cisplatin cytotoxicity by affecting glutathione synthesis or reactive oxygen species production [23-25]. However, the precise mechanisms by which copper ions modulate cisplatin sensitivity in liver cancer through specific signaling pathways remain unclear.

This study aims to investigate the expression pattern of ATOX1 in liver cancer and its relationship with clinical prognosis, elucidate the molecular mechanism of the ATOX1-copper axis in regulating cisplatin sensitivity in liver cancer, and develop small molecule inhibitors targeting ATOX1 through virtual screening and experimental validation to evaluate their anti-tumor effects in combination with cisplatin. This research will contribute to a deeper understanding of the molecular mechanisms underlying cisplatin resistance in liver cancer and may provide novel targets and strategies for precision treatment of liver cancer, offering significant theoretical and clinical translational value.

Results

ATOX1 was identified as a key regulator of cisplatin resistance in liver cancer via CRISPR/Cas9 library screen

To investigate key regulatory factors associated with cisplatin resistance in liver cancer cell lines, we employed genome-wide CRISPR-Cas9 screening technology to identify potential targets. We selected HepG2 and Huh7 liver cancer cell lines as research subjects. As shown (**Fig. 1A**), we first established HepG2 and Huh7 cell lines stably expressing Cas9 and successfully transfected them

with the TKOv3 sgRNA library. The experimental design included three key time points: day 0 as baseline control, followed by 21-day treatment with either DMSO (solvent control) or cisplatin. Results (**Fig. 1B-C**) displayed the distribution of the initial sgRNA library in both HepG2 and Huh7 cell lines and showed a typical left-skewed distribution with most sgRNA reads between 500-1000, indicating uniform library coverage as expected. KEGG pathway enrichment analysis of screening results (**Fig. 1D-E**) revealed significant enrichment of platinum drug resistance-related pathways in both cell lines. Through Venn diagram analysis (**Fig. 1F**), we identified 67 genes associated with cisplatin sensitivity common to both HepG2 and Huh7 cells. Previous studies suggested that certain genes mediated cisplatin resistance by enhancing DNA repair [26]. Consistent with these findings, our screening identified well-established DNA repair genes, such as *ERCC1* and *ERCC6*, positively correlated with cisplatin resistance, underscoring the reliability of our results (**Fig. 1F**). Beyond these well-known DNA repair genes, we identified *ATOX1* as one of the top 10 drug-resistant genes with the highest drugZ scores in both HepG2 and Huh7 cell lines (**Fig. 1G**). Further analysis of ATOX1 sgRNA dynamic changes (**Fig. 1H**) revealed that compared to baseline and DMSO groups, sgRNAs targeting ATOX1 were significantly reduced in the cisplatin treatment group. Moreover, we assessed ATOX1 protein expression in the human immortalized hepatocyte cell line THLE-2 and various liver cancer cell lines, including HepG2, Huh1, Hep3B, SNU449, JHH7, Huh7, Li-7, and SNU-475. The results showed that, compared to THLE-2, all liver cancer cells exhibited elevated ATOX1 expression (**Fig. 1I**). Specifically, ATOX1 expression was relatively low in HepG2, Huh1, Hep3B, and SNU449 cells, which were categorized as ATOX1 low-expression liver cancer cell lines, while ATOX1 expression was relatively high in JHH7, Huh7, Li-7, and SNU-475 cells, which were named ATOX1 high-expression liver cancer cell lines (**Fig. 1I**). Furthermore, through CCK-8 assays, we found that, compared to the ATOX1 low-expression liver cancer cell lines (with IC50 values ranging from 6 to 10 μM), the ATOX1 high-expression liver cancer cell lines (with IC50 values ranging from 11 to 16 μM) exhibited increased resistance to cisplatin (**Fig. 1J-K**). Overall, these results suggested that ATOX1 plays an important role in the cisplatin resistance mechanism of liver cancer.

High ATOX1 expression significantly correlates with poor prognosis and cisplatin resistance in liver cancer patients

To investigate the expression pattern of ATOX1 in liver cancer, we performed IHC analysis on cancer tissues and adjacent non-cancerous tissues from liver cancer patients. As shown (**Fig. 2A-B**), ATOX1 staining intensity was markedly higher in liver cancer tissues compared to adjacent tissues. Additionally, in 61.6% of paired samples, ATOX1 expression in liver cancer tissues was higher than in corresponding adjacent tissues (**Fig. 2C**). ROC curve analysis indicated that ATOX1 could serve as a potential biomarker for distinguishing liver cancer disease status (**Fig. 2D**) and recurrence risk (**Fig. 2E**). To further explore the relationship between ATOX1 expression and patient prognosis, we conducted survival analysis. Results showed that patients with high ATOX1 expression exhibited significantly reduced overall survival rates (**Fig. 2F**) and disease-free survival rate (**Fig. 2G**). Furthermore, we found that a nomogram model incorporating ATOX1 expression and some clinical traits had potential to predict 1-year, 3-year, and 5-year survival probabilities for liver cancer patients (**Fig. 2H**). These evidences indicated that high ATOX1 expression significantly correlates with poor prognosis.

Furthermore, through performing oncoPredict analysis in TCGA and ICGC database, we found that the high *ATOX1* expression group demonstrated higher cisplatin resistance scores (**Fig. 2I**). Correlation analysis further confirmed that *ATOX1* expression levels were significantly positively correlated with cisplatin resistance scores observed in both the TCGA dataset (**Fig. 2J**) and the ICGC dataset (**Fig. 2J**). In summary, these results indicated that ATOX1 was closely associated with cisplatin resistance.

ATOX1 reduces cisplatin sensitivity in liver cancer cells

To investigate the effects of *ATOX1* knockdown on cisplatin sensitivity in liver cancer cells, three targeting *ATOX1* siRNAs were used. qRT-PCR and western blotting assays indicated that si1-*ATOX1* exhibited the most efficiency to reduce the mRNA (**Fig. 3A**) and protein levels (**Fig. 3B**) of ATOX1. CCK-8assay results indicated knockdown of *ATOX1* significantly reduced the IC50 of cisplatin in HepG2 and Huh7 cells (**Fig. 3C**). Similarly, we constructed ATOX1 overexpressing

HepG2 and Huh7 cells (**Fig. 3D-E**). CCK-8 results indicated that overexpression of *ATOX1* increased the IC50 of cisplatin in HepG2 and Huh7 (**Fig. 3F**). Moreover, EdU staining further confirmed this result, with the percentage of EdU-positive cells in the *ATOX1* knockdown plus cisplatin treatment group being markedly lower than in the other three groups (**Fig. 3G**). Subsequently, we assessed the impact of different treatment modalities on the long-term proliferation capability of liver cancer cells *in vitro* through plate colony formation assays. As shown (**Fig. 3H**), compared to other treatment groups, the *ATOX1* knockdown combined with cisplatin treatment group exhibited significantly fewer colonies. Additionally, flow cytometry analysis revealed that the apoptosis rate in the *ATOX1* knockdown plus cisplatin treatment group was significantly higher than in the DMSO, si-*ATOX1*, or cisplatin treatment alone groups (**Fig. 3I**).

Similarly, we conducted a subcutaneous tumorigenesis assay to analyze the impact of *ATOX1* silencing on cisplatin sensitivity *in vivo*. It was demonstrated that HepG2 cells with *ATOX1* knockdown exhibited the slowest growth rate after cisplatin treatment (**Fig. 3J-L**). Moreover, we extracted tumor tissues derived from HepG2 cells and found that tumor tissues from HepG2 cells with *ATOX1* knockdown exhibited the lightest weight after cisplatin treatment (**Fig. 3M**). Furthermore, through IHC staining, we observed that tumor tissues from HepG2 cells with *ATOX1* knockdown showed the lowest expression of KI67 (**Fig. 3N**). In conclusion, these results demonstrate that *ATOX1* knockdown can significantly enhance the sensitivity of liver cancer cells to cisplatin, providing a potential new strategy for liver treatment.

Compound 8 identified as an efficient ATOX1-specific inhibitor with excellent binding affinity and pharmacokinetic properties

Based on the significant role of ATOX1 knockout in enhancing cisplatin sensitivity, we aim to develop relevant inhibitors. First, to identify key binding regions of the ATOX1 protein and discover potential inhibitors, we performed molecular dynamics simulations and large-scale virtual screening. Molecular dynamics simulations showed conformational changes of the ATOX1 protein at 0ns, 50ns, and 100ns time points (**Fig. 4A**), with the protein structure maintaining

relative stability throughout the simulation. Based on the analysis of the 100ns molecular dynamics trajectory, root mean square deviation (RMSD) values fluctuated mainly within the range of 0.5-1.5 Å (**Fig. 4B**), indicating that apo-ATOX1 was in a stable state. Residue fluctuation analysis (RMSF) revealed protein flexibility regions, showing lower fluctuations in the 18-30 residue interval and higher fluctuations in the 40-50 residue interval (**Fig. 4C**), which might be potential drug targeting sites.

Based on the above structural analysis, we performed virtual screening of 1.5 million compounds from the ChemDiv database using AutoDock-vina (**Fig. 4D**). We first selected the top 20% candidate compounds, then reduced the candidates to 12,000 through K-means clustering analysis. Further binding mode analysis reduced the number of compounds to 100, and finally, 62 compounds with potential ATOX1 inhibitory activity were identified and purchased through scaffold-specific screening (**Fig. 4D; Table 1**). As shown in **Table 1**, fluorescence spectroscopy analysis of these compounds and ATOX1 protein revealed that most compounds displayed low activity, with a recovery rate of less than 60%. However, four compounds, named compound 8, compound 25, compound 29, and compound 52, exhibited higher activity. Interestingly, these four compounds featured diverse scaffolds and functional groups compared to the known ATOX1 inhibitor, DC_AC50 (**Fig. 4E**). Among them, the known ATOX1 inhibitor, DC_AC50, exhibited a recovery rate of 98% (**Fig. 4F; Table 1**), while compound 8 showed a recovery rate of 95% (**Fig. 4F; Table 1**). In contrast, compound 25, compound 29, and compound 52 displayed recovery rates of 93%, 89%, and 78% (**Supplemental Fig. 1A; Table 1**), respectively. Therefore, we focused on compound 8 for further study.

After conducting a structural similarity search for the most active candidate compounds and purchasing 9 analogs **(Table 2)** to obtain compounds with better activity, we performed FRET experiments for verification. The results showed that analogs did not exhibit high recovery rates (**all < 60%; Fig. 4G**). SPR analysis confirmed the high-affinity binding of compound 8 to ATOX1, with a Kd value of 12.5μM (**Fig. 4H**). PTS experiments revealed the strongest signal of compound 8 for ATOX1 protein at 100 μM (**Fig. 4I**). To elucidate the potential mechanism of action of

compound 8 (#8), molecular docking studies were conducted to explore the interaction patterns between compound 8 and the positive control DC_AC50 to the ATOX1 protein. Results indicated that DC_AC50 penetrated deeply into the active pocket of ATOX1, forming stable hydrogen bonds and hydrophobic interactions with key residues, including LYS-60, LYS-25, ARG-21, and VAL-22 **(Supplemental Fig. 1B)**. Similarly, compound 8 effectively occupied the same binding site on ATOX1, establishing multiple intermolecular interactions with residues LYS-25, ARG-21, VAL-22, THR-54, and LYS-57 (**Fig. 4J**).These findings suggest that compound 8 binds to ATOX1 in a manner similar to DC-AC50, indicating its potential to modulate intracellular copper transport by targeting ATOX1. Previous studies indicated that copper chaperone for superoxide dismutase (CCS) protein is another target of DC_AC50 [27,28]. However, through performing molecular docking, compound 8 does not bind to the active pocket of CCS protein with a docking score greater than -7 **(Supplemental Fig. 1C).**

Moreover, molecular dynamics simulations showed that the 8/ATOX1 complex exhibited high conformational stability, with RMSD values mainly distributed in the 1.5-2.0 Å range **(Fig. 4K)**. Residue contribution analysis indicated that hydrophobic residues such as ASN23, VAL28, and LYS29 provided significant energy contributions to the 8/ATOX1 complex, with non-polar forces being the main contributing forces (**Fig. 4L**). Binding free energy analysis showed that both complexes possessed thermodynamic stability, but the 8/ATOX1 complex displayed stronger binding energy (**Fig. 4M**). Furthermore, ADMET analysis indicated that compound 8 performed well in terms of blood-brain barrier permeability (**Fig. 4N**). Overall, these results suggest that compound 8 is a highly specific ATOX1 inhibitor with excellent binding characteristics and drug potential.

ATOX1 inhibitor demonstrates significant synergistic anti-tumor effects with cisplatin on liver cancer cell

Before investigating the combined effect of compound 8 and cisplatin, we analyzed the individual effects of compound 8 and the known ATOX1 inhibitor DC_AC50 on liver cancer cells and immortalized hepatocyte THLE-2 using the CCK-8 assay. The results showed that the IC50 of

DC_AC50 for HepG2 and Huh7 cells were 9.5 μM and 10.2 μM, respectively, while for the immortalized hepatocyte line THLE-2, the IC50 was 34.2 μM (**Fig. 5A**). In comparison, compound 8 exhibited weaker inhibition against HepG2 and Huh7 cells with IC50 values of 16.5 μM and 22.0 μM, respectively (**Fig. 5A**). However, compound 8 showed lower non-specific toxicity to THLE-2, with an IC50 of 138.9 μM. These results suggest that compound 8 has superior selectivity index (SI; normal cell IC50/cancer cell IC50) compared to DC_AC50.

Then, we conducted a series of *in vitro* experiments on liver cancer cell lines HepG2 and Huh7 to investigate the synergistic anti-tumor effects of the compound 8 and cisplatin. Through performing CCK-8, we found that most combinations of compound 8 and cisplatin within the 0-10 μM range show a simple additive effect or weak synergistic effect in HepG2 and Huh7 cells (**Fig. 5B-C**). However, a combination of 10 μM compound 8 and 10 μM cisplatin demonstrates a moderate strong synergistic effect(**Fig. 5B-C**). Therefore, this combination was used for further study. EdU staining analysis **(Fig. 5D)** showed that the combination treatment group had a lower positive rate compared to the single-drug treatment groups. Additionally, plate colony formation assays **(Fig. 5E)** confirmed that the combination of compound 8 and cisplatin significantly reduced the colony formation ability of HepG2 and Huh7 cells compared to single-drug treatment groups. Moreover, flow cytometry analysis **(Fig. 5F)** results showed that compared to the control group and single-drug treatment groups, the apoptosis rate in the combination treatment group increased significantly. Overall, these results suggest that the combination of compound 8 and cisplatin demonstrates significant synergistic anti-tumor effects *in vitro*.

To evaluate the anti-tumor effects of ATOX1 inhibitor compound 8 alone and in combination with cisplatin in HepG2 xenograft models, we established subcutaneous transplantation tumor models and conducted a systematic study **(Fig. 5G)**. Tumor volume administrate **(Fig. 5H)** and optical *in vivo* imaging **(Fig. 5I)** showed that compared to the control group, both the cisplatin group and compound 8 group exhibited certain anti-tumor activity, while the combination treatment group demonstrated the most significant tumor inhibition effect. Tumor tissues obtained after the experiment further confirmed this result, with the tumor volume in the combination treatment

group being significantly smaller than in the other groups **(Fig. 5J)**. Meanwhile, immunohistochemical scoring results for the proliferation marker Ki67 and PCNA in tumor tissues indicated that compared to the tissues in control group and single drug treatment group, Ki67 and PCNA expression was significantly reduced in the tumor tissues in the combination treatment group (**Fig. 5K**).

To assess the potential toxicity of various treatment regimens on important organs, we performed HE staining on heart, liver, lung, kidney and gastrointestinal (GI) tract tissues. The results showed intact organ tissue structures in all treatment groups with no obvious pathological changes, further confirming the safety of the treatments (**Fig. 5L**). In conclusion, these results confirm that the compound 8 combined with cisplatin exhibits significant anti-tumor activity and good safety profile *in vivo*.

Targeted inhibition of ATOX1 by compound 8 increases DNA methylation at the NOTCH1 promoter in a copper-dependent manner

To investigate the mechanism by which compound 8 synergizes with cisplatin, we performed RNA-seq on HepG2 cells treated with DMSO, compound 8, cisplatin, or the combination of compound 8 and cisplatin. Principal component analysis revealed distinct clustering patterns among the treatment groups, indicating that each treatment elicited a unique global transcriptional response **(Fig. 6A)**. We next conducted DEG analysis. Compared with the DMSO control, treatment with compound 8 alone resulted in 196 DEGs (46 upregulated and 150 downregulated) (**Fig. 6B**). Treatment with cisplatin alone yielded 482 DEGs, including 175 upregulated and 307 downregulated genes (**Fig. 6B**). Notably, the combination treatment led to 546 DEGs, comprising 176 upregulated and 370 downregulated genes (**Fig. 6B**). We performed KEGG pathway enrichment analysis of the DEGs regulated by compound 8. The analysis revealed that these DEGs were predominantly enriched in pathways related to ATP-dependent chromatin remodeling, transcriptional misregulation, and the Notch signaling pathway (**Fig. 6C**). Notably, *NOTCH1* and *HES1*, two core components of the Notch pathway, were among the genes significantly downregulated upon treatment with compound 8 (**Fig. 6C**).

Multiple studies have shown that exposure to chemotherapeutic agents such as cisplatin activates the NOTCH signaling pathway in tumor cells. This activation can promote chemoresistance through multiple mechanisms, including enhancing stemness, strengthening DNA damage repair, increasing drug efflux, and conferring resistance to apoptosis [29,30]. Therefore, we performed GSEA analysis of NOTCH signaling for the gene changes induced by drugs. Consistent with previous reports, GSEA analysis results demonstrated that cisplatin treatment activated the NOTCH signaling pathway in HepG2 cells (NES = 1.78, P = 0.017; **Fig. 6D**). In contrast, treatment with compound 8 alone suppressed NOTCH pathway activation (NES = -1.45, P = 0.042; **Fig. 6D**). However, in the combination treatment group, the change in NOTCH pathway activity was not statistically significant compared with the control (NES = -1.14, P = 0.134; **Fig. 6D**). Collectively, these findings suggest that the ATOX1 inhibitor compound 8 may enhance the anti-tumor effect of cisplatin by counteracting the compensatory activation of NOTCH signaling induced by cisplatin, thereby potentiating cisplatin-mediated growth inhibition.

To validate the RNA-seq findings and further investigate how compound 8 suppresses activation of the NOTCH signaling pathway, we conducted a series of molecular biology experiments. First, we assessed the expression levels of NOTCH1 and HES1 in liver cancer cells in the NC and ATOX1 knockdown groups using qRT-PCR and western blotting. The results showed that, compared with NC cells, both the mRNA **(Fig. 6E)** and protein levels **(Fig. 6F)** of NOTCH1 and HES1 were significantly reduced in ATOX1-knockdown liver cancer cells. Similarly, through qRT-PCR (**Fig. 6G**) and western blotting (**Fig. 6H**), compound 8 reduced the mRNA and protein expression levels of NOTCH1 and HES1 in liver cancer cells in a concentration-dependent manner. Moreover, immunofluorescence staining **(Fig. 6I)** showed that treatment with compound 8 significantly reduced both the overall expression and nuclear localization of NOTCH1 protein in liver cancer cells. Taken together, these evidences indicated that targeting ATOX1 through either gene silencing or pharmacological approaches significantly suppresses the NOTCH1/HES1 signaling pathway.

Given that ATOX1 is a copper chaperone involved in copper transport, we next investigated whether ATOX1-mediated regulation of NOTCH1 is copper-dependent. To this end, we performed rescue experiments using 5 μM tetrathiomolybdate/ ammonium tetrathiomolybdate (TTM; copper chelator). The results showed that TTM treatment significantly alleviated the *ATOX1* knockdown–induced reduction in NOTCH1 and HES1 expression at both the mRNA (**Fig. 6J**) and protein levels (**Fig. 6K**). Previous studies indicated that intracellular copper levels can modulate DNA methylation patterns by regulating cellular redox homeostasis and influencing the activity of various epigenetic regulators. Dysregulated copper homeostasis may therefore contribute to aberrant promoter methylation, leading to altered gene transcription [31,32]. Therefore, we examined the DNA methylation status of the NOTCH1 promoter. The results showed that ATOX1 knockdown significantly increased NOTCH1 promoter methylation, whereas treatment with TTM (5 μM) markedly attenuated the hypermethylation induced by *ATOX1* depletion (**Fig. 6L**). Consistent with the effects observed following ATOX1 silencing by genetic approaches, we found that the ATOX1 inhibitor compound 8 increased intracellular copper levels (**Fig. 6M**) and enhanced DNA methylation (**Fig. 6N**) within the NOTCH1 promoter region in a concentration-dependent manner. Likewise, TTM treatment significantly suppressed compound 8–induced NOTCH1 promoter methylation (**Fig. 6O**), as well as the transcriptional repression (**Fig. 6P**) and reduced protein expression (**Fig. 6Q**) of NOTCH1 and HES1.

Taken together, our findings indicate that inhibition of ATOX1 through either gene silencing or pharmacological approaches elevates intracellular copper accumulation, which is associated with increased methylation of the *NOTCH1* promoter region, ultimately leading to transcriptional repression of *NOTCH1*.

The synergistic effect between compound 8 and cisplatin is dependent on the ATOX1/NOTCH1 axis.

To rule out the possibility that the modulation of the NOTCH1/HES1 signaling pathway by compound 8 and its synergistic effect with cisplatin are mediated through off-target effects, we conducted a series of experiments in *ATOX1*-silenced cells. Compound 8 (10 μM) was applied to

liver cancer cells with *ATOX1* knockdown. The results showed that compound 8 did not exert a significant effect on further increasing the methylation level of the *NOTCH1* promoter (**Fig. 7A**), nor did it further suppress the transcription of *NOTCH1* and its downstream target gene *HES1* in *ATOX1*-silenced liver cancer cells (**Fig. 7B**). Additionally, through western blotting analysis, we found that in NC cells, consistent with previous sequencing results, cisplatin treatment alone increased the expression of NOTCH1 and HES1 in liver cancer cells, while treatment with compound 8 alone inhibited the expression of both (**Fig. 7C**). When the two drugs were combined, their effects were mutually counteracted (**Fig. 7C**). However, in *ATOX1* knockout cells, we observed that compound 8 was unable to further reduce the expression of NOTCH1 and HES1, nor could it inhibit the cisplatin-induced upregulation of NOTCH1 and HES1 expression (**Fig. 7C**). Moreover, based on the colony formation assay (**Fig. 7D**) and the EdU incorporation assay (**Fig. 7E**), we found that compound 8 was unable to further reduce colony formation or the EdU-positive rate, and it did not exhibit a synergistic effect with cisplatin in liver cancer cells with *ATOX1* knockdown. These findings suggest that the synergistic effect of compound 8 with cisplatin is not mediated through off-target effects.

Furthermore, we investigated the role of NOTCH1 in the synergistic effect between compound 8 and cisplatin in liver cancer cells. *NOTCH1* overexpressing liver cancer cells were constructing (**Fig. 7F**). Through CCK-8 (**Fig. 7G**) and EdU assays (**Fig. 7H**), it was demonstrated that the combination of compound 8 and cisplatin exhibited strong inhibitory effects on the liver cancer cells transfected with vector. However, this combination therapy showed weaker inhibitory efficacy in *NOTCH1*-overexpressing liver cancer cells. Taken together, our evidences indicated that the synergistic effect between compound 8 and cisplatin is dependent on the ATOX1/NOTCH1 axis.

Material and methods

Liver cancer tissue specimens

A total of 60 liver cancer and paired adjacent non-tumor tissue specimens used in this study were

obtained from the Department of Pathology, Affiliated Hospital of Guizhou Medical University. All patients were pathologically confirmed to have liver cancer independently diagnosed by two pathologists. Tissue collection was approved by the Ethics Committee of the Affiliated Hospital of Guizhou Medical University and conducted in accordance with the principles of the Declaration of Helsinki. Written informed consent was obtained from all patients, and all ethical regulations relevant to human research participants were followed

Cell culture

Liver cancer cell lines HepG2 and Huh7 were purchased from the Cell Bank of the Chinese Academy of Sciences (Shanghai, China). The human immortalized hepatocyte cell line THLE-2, along with the liver cancer cell lines Huh1, Hep3B, JHH7, and Li-7, were sourced from Procell (Wuhan, China). Additionally, the liver cancer cell lines SNU-449 and SNU-475 were purchased from iCell (Shanghai, China). All cell lines were authenticated by STR profiling and tested for mycoplasma contamination to rule out any potential mycoplasma infection. All cells were cultured in DMEM medium (Gibco, USA) supplemented with 10% fetal bovine serum (FBS, Gibco, USA) and maintained in a humidified incubator at 37°C with 5% CO_2. All cell lines were authenticated by short tandem repeat profiling and tested for mycoplasma contamination and cell viability.

CRISPR-Cas9 library screen

Stable Cas9-expressing HepG2 and Huh7 liver cancer cell lines were constructed and transfected with the Toronto Knockout v3 (TKOv3) sgRNA library via a lentiviral system. After transfection, cells were divided into three groups: a baseline control group at day 0, a DMSO solvent control group, and a cisplatin treatment group for 21 days. At the end of the experiment, cells from each group were collected, and genomic DNA was extracted for high-throughput sequencing. DrugZ algorithms were used to analyze sgRNA abundance changes, identify genes significantly affecting cisplatin sensitivity ($P<0.05$), and perform KEGG pathway enrichment analysis. Venn diagram analysis was used to compare genes associated with cisplatin sensitivity in both HepG2 and Huh7 cell lines.

siRNA and lentiviral transfection

Negative control (NC) and siRNA sequences targeting *ATOX1* were designed and synthesized by GenePharma (Shanghai, China). siRNA sequences used were showed as follows: 5'-UUCUCCGAACGUGUCACGUTT-3' (NC), 5'-GCAGCUGAACCUGACAACUTT-3' (si1-*ATOX1*), 5'-GCAACAAGAAGGUGCUGAUTT-3' (si2-*ATOX1*) and 5'-CAGGAAAGACUGUUUCCUACC-3' (si3-*ATOX1*). siRNA transfection was performed using Lipofectamine RNAiMAX reagent (Invitrogen, USA) according to the manufacturer's instructions. Transfection efficiency was verified by RT-qPCR and western blotting. For lentiviral packaging, pLKO.1-puro (Addgene plasmid #8453) and pLenti CMV/TO Puro empty (Addgene plasmid #17482) were obtained from Addgene (USA). The ATOX1-targeting shRNA was carried in the pLKO.1-puro backbone; the target sequence was 5′-GCAGCTGAACCTGACA ACT-3′. The CDS of ATOX1 (RefSeq NM_004045) and NOTCH1 (RefSeq NM_017617.5) were carried into pLenti CMV/TO Puro empty to package ATOX1 and NOTCH1 overexpressing lentiviral. All lentiviral packaging procedures were performed according to protocols provided by Addgene. Lentiviral were transfected into liver cancer cells using Polybrene (Invitrogen, USA). Stable *ATOX1* knockdown and gene overexpressing cell lines were generated by selecting with 0.5 μg/mL puromycin (MCE, Wuhan, China) for 14 consecutive days.

Bioinformatics Analysis

Gene expression and clinical data of liver cancer patients were downloaded from the TCGA-LIHC and ICGC databases. Data processing and analysis were performed using R software (v4.0.3) and Bioconductor packages. Patients were divided into high-expression and low-expression groups based on the median expression level of *ATOX1*. OncoPredict algorithm (version: 1.2) was used to analyze drug resistance score of 198 drugs in the liver cancer tissues from TCGA and ICGC database. The difference of cisplatin resistance score between high *ATOX1* and low *ATOX1* group liver cancer tissues were analyzed by un-pair t-test, while the co-express relationship between *ATOX1* expression and cisplatin resistance score was analyzed by Pearson co-expression analysis.

Molecular Dynamics Simulation and Virtual Screening

The ATOX1 protein structure (PDB ID: 1FEE) was obtained from the Protein Data Bank (PDB). The protein structure was optimized using SYBYL-X2.0 software, including hydrogen addition, charge assignment, and energy minimization. Molecular dynamics simulations were performed using AMBER20 for 100 ns. The AMBER99SB force field was used with the TIP3P water model under periodic boundary conditions. The system was equilibrated at 300K temperature and 1 bar pressure, with long-range electrostatic interactions calculated using the Particle Mesh Ewald method. A time step of 2 fs was used, and conformations were saved every 10 ps for subsequent analysis. Virtual screening of 1.5 million compounds from the ChemDiv database was performed using AutoDock-vina software. Candidate compounds ranked in the top 20% based on binding energy scores were selected, and structural diversity analysis was performed using the K-means clustering algorithm. A total of 100 candidate compounds were further selected for experimental validation through molecular docking analysis.

ADMET Analysis

The pharmacokinetic properties of compound 8 and other compounds, including absorption, distribution, metabolism, excretion, and toxicity parameters, were predicted using the SwissADME online tool (http://www.swissadme.ch) and the pkCSM online platform (http://biosig.unimelb.edu.au/pkcsm).

Protein Purification

ATOX1 and celwy plasmids were transformed into BL21(DE3) cells and cultured in medium containing kanamycin. After sequence verification, protein expression was induced with 0.1 mM IPTG at 16°C for 14-16 hours. Collected cells were lysed by sonication, and the supernatant was purified via nickel affinity chromatography using step elution (10-50% Buffer C). The target protein was analyzed by SDS-PAGE, buffer-exchanged into 20 mM HEPES pH 7.1, 100 mM NaCl, 1 mM DTT, and further purified via Superdex 75 gel filtration. Purified protein was quantified by comparison with BSA standards and stored at -80°C.

Fluorescence Resonance Energy Transfer (FRET) Assay

A FRET system based on ATOX1_WD4 and copper ion binding was used to evaluate the inhibitory effect of compounds on ATOX1-copper ion binding. Plasmids containing CFP-ATOX1-YFP fusion proteins were transfected into HEK293T cells. Forty-eight hours post-transfection, cells were incubated with different concentrations of candidate compounds (0-100 μM) for 2 hours. Fluorescence intensities of CFP (excitation 430 nm, emission 475 nm) and YFP (excitation 430 nm, emission 530 nm) were measured using a SpectraMax M5 multimode microplate reader (Molecular Devices, USA). FRET efficiency (FRET ratio = YFP emission/CFP emission) was calculated and dose-response curves were plotted.

Protein Thermal Shift (PTS) Assay

ATOX1 protein was thawed on ice and diluted to 1 mg/mL in PBS buffer (pH 7.4). Compound 8 was prepared at concentrations of 10, 25, 50, and 100 μM. Reaction mixtures (10 μL) contained 5 μL protein solution, 4 μL compound solution, and 1 μL SYPRO Orange dye (5000×), resulting in a final protein concentration of 0.5 mg/mL and dye concentration of 2.5×. Samples were loaded in triplicate into a 96-well PCR plate, sealed after appropriate controls were set. Thermal denaturation was performed from 25°C to 95°C at a rate of 0.5°C/min, with initial equilibration for 2 minutes and fluorescence values recorded every 0.2°C (excitation/emission: 485/580 nm). Melting temperatures (Tm) were determined using instrument software and analyzed with GraphPad Prism.

Surface Plasmon Resonance (SPR) Analysis

SPR analysis was performed using a Biacore X100 system. Purified ATOX1 protein was immobilized onto a CM5 chip (~2000 RU). Compound 8 was injected over the chip surface at ascending concentrations (0.625-10 μM) with a flow rate of 30 μL/min, contact time of 120 seconds, and dissociation time of 300 seconds. PBS with 1% DMSO was used as the running buffer. Equilibrium dissociation constants (Kd) were calculated using BiaEvaluation software (v4.1).

Quantitative Real-Time PCR (qRT-PCR)

Total RNA in liver cancer cells was extracted from cells using TRIzol reagent (Invitrogen, USA). cDNA was synthesized using the PrimeScript RT reagent kit (Takara, Japan). qRT-PCR was

performed using SYBR Green PCR Master Mix (Takara, Japan) on an ABI 7500 real-time PCR system (Applied Biosystems, USA). *GAPDH* was used as an internal reference gene, and relative expression levels were calculated using the $2^{\wedge(-\Delta\Delta CT)}$ method. Primer sequences were as follows: *ATOX1*-F: 5'-GTGCTGAAGTACGAGTTCTGC-3', *ATOX1*-R: 5'-GCTTGTCGTACTCCTCAGGG-3', *NOTCH1*-F: 5'-CGGGTCCACCAGTTTGAATG-3', *NOTCH1*-R: 5'-GTTGTATTGGTTCGGCACCAT-3', *HES1*-F: 5'-TCAACACGACACCGGATAAAC-3', *HES1*-R: 5'-GCCGCGAGCTATCTTTCTTCA-3', *GAPDH*-F: 5'-GGAGCGAGATCCCTCCAAAAT-3', and *GAPDH*-R: 5'-GGCTGTTGTCATACTTCTCATGG-3'. The experiment was repeated three times.

Western Blotting Analysis

Liver cancer cells were lysed in RIPA lysis buffer (50 mM Tris-HCl pH 7.4, 150 mM NaCl, 1% Triton X-100, 0.1% SDS) supplemented with protease inhibitor cocktail (Roche, Switzerland). Protein concentration was determined using a BCA protein assay kit (Thermo Fisher, USA). Equal amounts of protein samples (30 μg) were separated by SDS-PAGE and transferred to PVDF membranes (Millipore, USA). Membranes were blocked with 5% skim milk in TBST for 1 hour and incubated overnight at 4°C with primary antibodies: anti-ATOX1 (1:1000, Abcam, ab154179), anti-NOTCH1 (1:1000, CST, 3608), anti-HES1 (1:1000, CST, 11988), and anti-GAPDH (1:5000, Proteintech, 60004-1-Ig). The next day, membranes were incubated with horseradish peroxidase-conjugated secondary antibodies (1:5000, Proteintech) at room temperature for 1 hour. Chemiluminescent detection was performed using ECL reagent (Millipore, USA), and densitometric analysis was conducted using ImageJ software (NIH, USA). The experiment was repeated three times.

Cell Proliferation Assays

Liver cancer cell proliferation was detected by CCK-8, EDU and colony formation assays. For CCK-8 method, HepG2 and Huh7 cells were seeded at a density of 5×10^3 cells per well in 96-well plates and cultured for 24 hours before treatment. At designated time points after treatment, 10 μL of CCK-8 reagent (Dojindo, Japan) was added to each well and incubated at 37°C for 2

hours. Absorbance at 450 nm was measured using a microplate reader. Each group was set in triplicate, and experiments were independently repeated three times.

For EDU assays, HepG2 and Huh7 cells were seeded at a density of 2×10^4 cells per well in 24-well plates and cultured for 24 hours before treatment. After treatment, EdU incorporation was detected using the Cell-Light EdU Apollo 567 In Vitro Kit (RiboBio, China). After fixation, cells were incubated with Apollo dye solution for 30 minutes and stained with DAPI (1:1000) for 10 minutes. Fluorescent images were captured, and the percentage of EdU-positive cells was calculated by randomly selecting five fields of view. The experiment was repeated three times.

For colony formation assay, cells were seeded at a density of 1000 cells per well in 6-well plates and cultured for 24 hours before treatment. After treatment, cells were cultured for an additional 14 days with medium changes every 3 days. Colonies were fixed with 4% paraformaldehyde for 20 minutes and stained with 0.1% crystal violet for 15 minutes. The number of colonies containing more than 50 cells was counted. The experiment was repeated three times.

Flow Cytometry Analysis

Cell apoptosis was detected using the Annexin V-FITC/PI Apoptosis Detection Kit (BD Biosciences, USA). Cells were collected, washed twice with cold PBS, and resuspended in 100 μL binding buffer. Annexin V-FITC (5 μL) and PI (5 μL) were added, and cells were incubated at room temperature in the dark for 15 minutes. After adding 400 μL binding buffer, cells were analyzed using a BD FACSCanto II flow cytometer (BD Biosciences, USA). Data were analyzed using FlowJo software (v10.6.2). The experiment was repeated three times.

Drug Synergy Analysis

HepG2 and Huh-7 cells were treated with different concentrations of compound 8 (0, 2.5, 5, 10 μM) and cisplatin (0, 2.5, 5, 10 μM) alone or in combination for 48 hours. Cell viability was measured using the CCK-8 assay, and the combination index (CI) was calculated using CompuSyn software (ComboSyn Inc, USA) to evaluate drug synergy. $CI < 0.9$ indicated synergy, $0.9 \leq CI \leq 1.1$ indicated additivity, and $CI > 1.1$ indicated antagonism.

Animal Experiments

For animal experiments, a total of 48 BALB/c nude mice (6-8 weeks old, 18-22 g, female: male = 1/1) were purchased from Tianqin Biotechnology Co., Ltd. (Changsha, China). The experiment was approved by the Animal Ethics Committee of Guizhou Medical University with approval number as 2500097. After purchase, the animals were acclimated for 5 days in a specific pathogen-free (SPF) individual ventilated cage (IVC) system before being used for subsequent animal experiments. Prior to initiating the animal studies, inclusion criteria were defined in advance: (1) following the acclimation period, mice had body weights within the expected range for the strain; (2) for the subcutaneous xenograft experiments, the intended implantation site was intact and free of lesions, signs of infection, or other skin abnormalities. Animals that died before the planned endpoint or failed to develop tumors were excluded from the analysis. Throughout the study, mice were housed in a SPF grade IVC system under controlled conditions (22–25 °C, 40–60% humidity, 12-h light/dark cycle). Animals had free access to an irradiated pelleted diet and autoclaved ultrapure water, and bedding was replenished weekly.

In the experiments assessing whether *ATOX1* knockdown enhances cisplatin sensitivity, nude mice were randomized using a random-number table into four groups: NC + DMSO, NC + cisplatin, sh-*ATOX1* + DMSO, and sh-*ATOX1* + cisplatin. Five mice per group were pre-specified for analysis, with one additional mouse allocated to each group (six mice initially per group) to compensate for potential attrition due to unexpected death or failure of tumor establishment. Subcutaneous xenograft tumors were generated by injecting 5×10^6 NC HepG2 cells or *ATOX1*-knockdown HepG2 cells into the right axillary region. Treatment was initiated on day 8 after implantation, and mice received either DMSO or cisplatin (5 mg/kg, intraperitoneally, twice weekly).

In the experiments investigating the combined effects of compound 8 and cisplatin, a total of 24 nude mice were used. Each mouse was subcutaneously inoculated with 5×10^6 HepG2 cells. Tumor volumes were measured on day 7, and the four mice with the largest outlying tumor volumes were excluded. The remaining mice were then randomized using a random-number table into four groups (n = 5 per group): DMSO, compound 8 (10 mg/kg, intraperitoneal injection, once

daily), cisplatin (5 mg/kg, intraperitoneal injection, twice weekly), and the combination treatment (same doses as single agents).

Tumor volume was measured every 2 days using the formula: Volume (mm^3) = 0.5 × length × $width^2$, the health status of the nude mice was monitored daily. The experiments were considered complete when the tumor volume in one of the groups approaches 1000 mm^3. Then, mice were euthanized by carbon dioxide inhalation, and tumor tissues and major organs were collected for HE stain. Tumor fluorescence imaging was performed using the IVIS® Spectrum in vivo imaging system (PerkinElmer, USA). Fifteen minutes after intraperitoneal injection of luciferin (150 mg/kg), imaging was conducted under isoflurane anesthesia. Fluorescence signal intensity was analyzed using LivingImage software (v4.5).

Histological Analysis

For HE staining, tissue sections were fixed in 4% paraformaldehyde for 24 hours, dehydrated in graded ethanol, embedded in paraffin, and sectioned at 4 μm. After routine HE staining, tissue morphological changes were observed under an optical microscope.

For immunohistochemistry (IHC) Staining, tissue sections were deparaffinized and hydrated, followed by antigen retrieval in citrate buffer (pH 6.0) for 15 minutes via microwave treatment. Endogenous peroxidase activity was blocked with 3% H_2O_2 for 15 minutes, and sections were blocked with 5% goat serum for 30 minutes before overnight incubation at 4°C with anti-ATOX1 antibody (1:200, Abcam, ab154179), anti-Ki67 antibody (1:1000, CST, 9449) and anti-PCNA (1:6000, CST, 13110). The next day, sections were incubated with HRP-conjugated secondary antibody at room temperature for 30 minutes, visualized with DAB, counterstained with hematoxylin, and mounted with neutral gum. Semi-quantitative analysis was performed using Image-Pro Plus 6.0 software to calculate the integrated optical density (IOD) of positive staining.

Transcriptome Sequencing and Analysis

Total RNA was extracted from HepG2 cells subjected to different treatments. cDNA libraries were constructed and sequenced on the Illumina NovaSeq 6000 platform. Clean reads were aligned to the reference genome using HISAT2, and FPKM values for each gene were calculated using

StringTie. Following by normalizing $\log_2$ FPKM+1, differentially expressed genes were identified using limma package (version: 2.7) with the threshold as |FC| > 1.5 and p value < 0.05. KEGG enrichment analyses were performed using the clusterProfiler package (version: 3.18.1), and GSEA software (version: 4.1.0) was used for gene set enrichment analysis based on 1000 permutations, with a significance threshold of $P < 0.05$.

Immunofluorescence Staining

Cells were seeded on glass coverslips, fixed with 4% paraformaldehyde for 15 minutes after treatment, permeabilized with 0.5% Triton X-100 for 10 minutes, and blocked with 5% BSA for 1 hour. Cells were incubated overnight at 4°C with anti-NOTCH1 antibody (1:100, CST, 3608), followed by incubation with Alexa Fluor 647-conjugated secondary antibody (1:200, Invitrogen) at room temperature for 1 hour. Nuclei were stained with DAPI for 5 minutes. Images were captured under a confocal microscope.

Detection of NOTCH1 Gene Promoter Methylation

First, genomic DNA was extracted from cells in each treatment group. A total of 500 ng of DNA was treated with the EZ DNA Methylation-Gold™ Kit (Zymo Research) for bisulfite conversion, which converts unmethylated cytosines to uracil, while methylated cytosines remain unchanged. The specific conversion protocol was as follows: incubate at 98°C for 10 minutes, then at 64°C for 2.5 hours. After conversion, the DNA underwent a series of purification steps, including DNA binding, washing, and desulfonation, and was finally eluted with an elution buffer to a concentration of 20 ng/μL.

Based on the CpG island sequence in the *NOTCH1* promoter region (NCBI reference sequence), two sets of specific primers were designed for qMSP detection: Methylation-specific primers: forward primer: 5'-TTTTTTTTAGTTTTTCGGTTTTTTC-3'; reverse primer: 5'-CAAAATACCTACCATAATCCCTACG-3', and non-methylation-specific primers: forward primer: 5'-TTTTTTAGTTTTTTGGTTTTTTTGT-3', reverse primer: 5'-AAATACCTACCATAATCCCTACACA-3'. The qPCR reaction system was 20 μL, consisting of 10 μL of 2×SYBR Green Master Mix, 0.4 μL of each forward and reverse primer (10 μM), 2 μL

of the converted DNA template (approximately 40 ng), and ddH_2O to make up the volume. The amplification conditions were: 95°C for 10 minutes for initial denaturation, followed by 40 cycles of amplification (95°C for 15 seconds, 60°C for 1 minute). Three technical replicates were performed for each sample, and the *GAPDH* gene was used to normalize DNA template quantity variations.

The methylation level of the *NOTCH1* promoter was expressed as the PMR (percentage of methylated reference) value, calculated as follows: PMR = [the ratio of methylated *NOTCH1* to *GAPDH* in the sample / the ratio of fully methylated positive control] × 100%. The experiment was repeated three times.

Statistical Analysis

All data were analyzed using GraphPad Prism 8.0 software (GraphPad Software, USA). Data are expressed as mean ± standard deviation (SD). Student's t-test was used for comparisons between two groups, and one-way ANOVA followed by Tukey's multiple comparisons was used for comparisons among multiple groups. Survival analysis was performed using the Kaplan-Meier method, and differences between groups were assessed using the log-rank test. Correlation analysis was conducted using Pearson or Spearman correlation coefficients. A p-value < 0.05 was considered statistically significant. All experiments were independently repeated at least three times.

Discussion

This study reveals for the first time the critical role of the ATOX1-copper ion-NOTCH signaling axis in regulating cisplatin sensitivity in liver cancer cells and successfully develops a small molecule inhibitor named compound 8 (#8) targeting ATOX1, providing a novel therapeutic strategy for overcoming chemotherapy resistance in liver cancer.

Cisplatin resistance remains one of the major challenges in cancer therapy. Over the past few decades, researchers have developed multiple targeting strategies to overcome this resistance. These approaches primarily address several key aspects: targeting platinum drug transport, such

as increasing the expression of CTR1 or inhibiting the function of ATP7A/B [33,34]; inhibiting DNA repair mechanisms, with targets including ERCC1, BRCA1/2, and others [35]; targeting apoptosis regulators like p53 and Bcl-2 family proteins; and modulating epigenetic changes including DNA methylation and histone modifications [36,37]. However, these strategies have notable limitations: drugs targeting transport systems often lack specificity, leading to severe side effects; DNA repair inhibitors may induce genomic instability, raising the risk of secondary malignancies; the effectiveness of apoptosis-regulating drugs is heavily dependent on the tumor cell's genetic background; and epigenetic-modulating drugs suffer from insufficient tissue specificity [38,39]. Additionally, these strategies typically target individual pathways, overlooking the complexity of tumor resistance mechanisms and the interactions among various signaling pathways.

In our study, we first identified ATOX1, a key protein involved in copper ion homeostasis, as being associated with cisplatin resistance in liver cancer cell through CRISPR/CAS9 library screening. Further analysis of clinical patient data revealed that ATOX1 expression was correlated with poor patient prognosis. Additionally, we found that knockdown of *ATOX1* increases copper ion accumulation and enhances the methylation level of the *NOTCH1* promoter region, thereby inhibiting NOTCH1 transcription and increasing the sensitivity of liver cancer cells to cisplatin. Unlike previous studies that suggest ATOX1 exports cisplatin as a substrate out of the cell, our research offers a novel perspective by interpreting ATOX1-mediated cisplatin resistance through the lens of "ion homeostasis-epigenetic modification." This expands the understanding of cisplatin resistance mechanisms, particularly the crosstalk between various resistance pathways

Currently, various drugs targeting cisplatin resistance are in clinical use or under investigation. For example, PARP inhibitors like Olaparib enhance cisplatin efficacy by inhibiting DNA repair but may cause severe side effects such as myelosuppression [40]. Bcl-2 inhibitors like Venetoclax can enhance cisplatin-induced apoptosis, but their effectiveness depends on the expression pattern of Bcl-2 family proteins in tumors [41]. While these drugs can enhance cisplatin sensitivity to some

degree, they generally suffer from insufficient specificity, significant side effects, or limited applicable populations.

Notably, although the importance of copper metabolism in tumor development and drug resistance is increasingly recognized, the development of specific drugs targeting the copper chaperone protein ATOX1 remains in its early stages. Some copper chelators like TTM and copper complexes such as Casiopeinas demonstrate antitumor activity, but their mechanisms of action are complex, making it difficult to distinguish therapeutic effects and toxic side effects [42].

Based on ATOX1's important role in the cisplatin resistance of liver cancer, we identified key binding regions of the ATOX1 protein and developed a highly specific ATOX1 inhibitor named compound 8 through molecular dynamics simulation and large-scale virtual screening. Compound 8 exhibits high targeting specificity, directly binding to the key functional domains of ATOX1 with a Kd value of 12.5 μM. In addition, it demonstrates favorable pharmacokinetic properties, including good solubility, membrane permeability, and metabolic stability, making it well suited for *in vivo* applications. Both *in vitro* and *in vivo* studies further confirm that, when combined with cisplatin, this inhibitor produces significant synergistic anti-liver cancer effects while maintaining a favorable safety profile.

To further evaluate the specificity of our ATOX1 inhibitor, we compared the newly developed compound 8 with the previously reported ATOX1 inhibitor DC_AC50. We found that, unlike DC_AC50, which targets both ATOX1 and CCS. Compound 8 does not interact with CCS, even though exhibiting a binding mode to ATOX1 similar to that of DC_AC50. These findings indicate the higher binding specificity of compound 8 toward ATOX1 and suggest that its nonspecific toxic side effects may be reduced compared with those of DC_AC50. This hypothesis was further supported by CCK-8 assays, which showed that although compound 8 alone exhibited slightly weaker anti–liver cancer activity than DC_AC50, it displayed a higher selectivity index and markedly lower cytotoxicity toward normal hepatocyte THLE-2. Collectively, these results highlight a potential therapeutic advantage of compound 8.

The NOTCH signaling pathway, as a highly conserved intercellular communication mechanism, plays important roles in the occurrence, development, and drug resistance of various tumors. Recent studies indicate that abnormal activation of the NOTCH signaling pathway is closely related to chemotherapy resistance in multiple tumors [43]. In pancreatic cancer, NOTCH1 activation promotes gemcitabine resistance by upregulating multidrug resistance-related proteins and P-glycoprotein [44]. In breast cancer, the NOTCH signaling pathway leads to doxorubicin resistance by maintaining cancer stem cell characteristics and upregulating anti-apoptotic proteins [45]. In liver cancer, NOTCH1 overexpression promotes sorafenib resistance by activating the PI3K/AKT/mTOR signaling pathway and inhibiting cell apoptosis [46]. Particularly noteworthy is the complex interaction between the NOTCH signaling pathway and the DNA damage repair (DDR) system. Studies show that NOTCH1 can enhance DNA repair capacity by regulating the expression of key DDR components such as ATM, BRCA1, and RAD51, thereby promoting tumor cell resistance to DNA-damaging agents like cisplatin [47]. Additionally, NOTCH signaling can participate in tumor resistance processes through various mechanisms such as regulating epithelial–mesenchymal transition, autophagy, and metabolic reprogramming [48]. Therefore, targeting the NOTCH signaling pathway is considered a potential strategy for overcoming tumor resistance.

In our research, we found that compound 8 can modulate copper ion homeostasis, leading to increased DNA methylation in the promoter region of NOTCH1 and consequent suppression of NOTCH signaling. Based on this mechanism, we hypothesize that compound 8 may exhibit synergistic effects when combined with a broader range of chemotherapeutic agents beside cisplatin, which could represent an additional therapeutic advantage. Nevertheless, this hypothesis requires further validation through additional experimental studies.

In conclusion, our research not only develops a promising new strategy for overcoming liver cancer cisplatin resistance but also provides a new perspective for understanding the interaction between copper metabolism and tumor signaling pathways, laying a foundation for more effective individualized liver cancer treatment in the future.

Ethics approval and consent to participate

The collection and use of liver cancer samples were approved by the Human Ethics Committee of Guizhou Medical University (approval number: 2021–255), and all participants provided written informed consent. Animal experiments was approved by the Animal Ethics Committee of Guizhou Medical University (Ethics Approval No. 2500097). All animal experiments were conducted in strict accordance with the guidelines and regulations of the committee to ensure the welfare and ethical treatment of animals involved in the research.

Consent for publication

All authors consent to the publication of this manuscript. Individual data included in this study are anonymized.

Acknowledgements and Funding

This research was financially supported by the National Natural Science Foundation of China (82560795 , 82260535), Guizhou Provincial Science and Technology Projects General (ZK[2026]341). We would like to thank the Figdraw platform (https://www.figdraw.com/#/) for providing the original materials and authorization approval for the creation of the schematic diagrams for Figure 1A and Figure 5G. The authorization approval numbers are TWWYA9335b and UWPIIde6be, respectively.

Availability of data and material

The raw FASTQ files from the CRISPR/Cas9 library screen and RNA-seq have been deposited in the CNCB database (https://www.cncb.ac.cn/) under accession number PRJCA056149. All other raw data are provided in the Supplementary Data and are available from the corresponding author upon reasonable request.

Competing interests

The authors declare no competing financial or non-financial interests.

Author contributions

Dan Ma, Shi Zuo, Lei Tang and Zhirui Zeng designed or supported the research and revised the manuscript. Chujiao Hu wrote the paper. Chujiao Hu, Huading Tai, Renguang Zhu, and Zhirui

Zeng performed the research and analyzed the data. Chujiao Hu, Huading Tai, Renguang Zhu, Zhirui Zeng, Zhengyu Shu and Guanghao Guo participated in animal experiments All the authors have read and approved the final version of the manuscript.

Reference

1. Bray, F. *et al.* Global cancer statistics 2022: GLOBOCAN estimates of incidence and mortality worldwide for 36 cancers in 185 countries. *CA Cancer J. Clin.* **74**, 229–263 (2024).
2. Rumgay, H. *et al.* Global burden of primary liver cancer in 2020 and predictions to 2040. *J. Hepatol.* **77**, 1598–1606 (2022).
3. Oh, J. H. & Jun, D. W. The latest global burden of liver cancer: a past and present threat. *Clin. Mol. Hepatol.* **29**, 355–357 (2023).
4. Forner, A., Reig, M. & Bruix, J. Hepatocellular carcinoma. *Lancet* **391**, 1301–1314 (2018).
5. Feng, F. & Zhao, Y. Hepatocellular carcinoma: prevention, diagnosis, and treatment. *Med. Princ. Pract.* **33**, 414–423 (2024).
6. Dasari, S. & Tchounwou, P. B. Cisplatin in cancer therapy: molecular mechanisms of action. *Eur. J. Pharmacol.* **740**, 364–378 (2014).
7. Galluzzi, L. *et al.* Molecular mechanisms of cisplatin resistance. *Oncogene* **31**, 1869–1883 (2012).
8. Siddik, Z. H. Cisplatin: mode of cytotoxic action and molecular basis of resistance. *Oncogene* **22**, 7265–7279 (2003).
9. Petruzzelli, R. & Polishchuk, R. S. Activity and trafficking of copper-transporting ATPases in tumor development and defense against platinum-based drugs. *Cells* **8**, 108 (2019).
10. Li, Y. Q. *et al.* Copper efflux transporters ATP7A and ATP7B: novel biomarkers for platinum drug resistance and targets for therapy. *IUBMB Life* **70**, 183–191 (2018).
11. Boal, A. K. & Rosenzweig, A. C. Crystal structures of cisplatin bound to a human copper chaperone. *J. Am. Chem. Soc.* **131**, 14196–14197 (2009).
12. Itoh, S. *et al.* Novel role of antioxidant-1 (Atox1) as a copper-dependent transcription factor involved in cell proliferation. *J. Biol. Chem.* **283**, 9157–9167 (2008).

13. Blockhuys, S., Zhang, X. & Wittung-Stafshede, P. Single-cell tracking demonstrates copper chaperone Atox1 to be required for breast cancer cell migration. *Proc. Natl Acad. Sci. USA* **117**, 2014–2019 (2020).
14. Zhao, X. *et al.* Expression of cuproptosis-related genes in hepatocellular carcinoma and their relationships with prognosis. *Front. Oncol.* **12**, 992468 (2022).
15. Boal, A. K. & Rosenzweig, A. C. Structural biology of copper trafficking. *Chem. Rev.* **109**, 4760–4779 (2009).
16. Palm-Espling, M. E. *et al.* Determinants for simultaneous binding of copper and platinum to human chaperone Atox1: hitchhiking not hijacking. *PLoS ONE* **8**, e70473 (2013).
17. Arnesano, F. *et al.* Characterization of the binding interface between the copper chaperone Atx1 and the first cytosolic domain of Ccc2 ATPase. *J. Biol. Chem.* **276**, 41365–41376 (2001).
18. Palm, M. E. *et al.* Cisplatin binds human copper chaperone Atox1 and promotes unfolding in vitro. *Proc. Natl Acad. Sci. USA* **108**, 6951–6956 (2011).
19. Safaei, R. *et al.* Role of copper transporters in the development of resistance to platinum drugs. *J. Inorg. Biochem.* **98**, 1607–1613 (2004).
20. Xie, J., Yang, Y., Gao, Y. & He, J. Cuproptosis: mechanisms and links with cancers. *Mol. Cancer* **22**, 46 (2023).
21. Kong, R. & Sun, G. Targeting copper metabolism: a promising strategy for cancer treatment. *Front. Pharmacol.* **14**, 1203447 (2023).
22. Huang, X., Lian, M. & Li, C. Copper homeostasis and cuproptosis in gynecological cancers. *Front. Cell Dev. Biol.* **12**, 1459183 (2024).
23. Li, Z. H. *et al.* Role of copper transporter ATP7A in platinum resistance of esophageal squamous cell carcinoma. *J. Cancer* **7**, 2085–2092 (2016).
24. Guan, D. *et al.* Copper in cancer: from pathogenesis to therapy. *Biomed. Pharmacother.* **163**, 114791 (2023).
25. Li, J. L. & Harris, A. L. Notch signaling from tumor cells: a new mechanism of angiogenesis. *Cancer Cell* **8**, 1–3 (2005).

26. Maharati, A. & Moghbeli, M. Forkhead box proteins as critical regulators of cisplatin response in tumor cells. *Eur. J. Pharmacol.* **956**, 175937 (2023).
27. Inkol, J. M., Poon, A. C. & Mutsaers, A. J. Inhibition of copper chaperones sensitizes human and canine osteosarcoma cells to carboplatin chemotherapy. *Vet. Comp. Oncol.* **18**, 559–569 (2020).
28. Wang, J. *et al.* Inhibition of human copper trafficking by a small molecule attenuates cancer cell proliferation. *Nat. Chem.* **7**, 968–979 (2015).
29. Fu, L. *et al.* Current research on the Notch pathway in hepatocellular carcinoma. *Eur. J. Med. Res.* **30**, 402 (2025).
30. Sosa Iglesias, V. *et al.* Drug resistance in non-small cell lung cancer: a potential for NOTCH targeting? *Front. Oncol.* **8**, 267 (2018).
31. Elkin, E. R. *et al.* Metals exposures and DNA methylation: current evidence and future directions. *Curr. Environ. Health Rep.* **9**, 673–696 (2022).
32. Santos, D. *et al.* Microplastics- and copper-induced changes in neurogenesis and DNA methyltransferases in early life stages of zebrafish. *Chem. Biol. Interact.* **363**, 110021 (2022).
33. Makovec, T. Cisplatin and beyond: molecular mechanisms of action and drug resistance development in cancer chemotherapy. *Radiol. Oncol.* **53**, 148–158 (2019).
34. Howell, S. B. *et al.* Copper transporters and the cellular pharmacology of platinum-containing cancer drugs. *Mol. Pharmacol.* **77**, 887–894 (2010).
35. Lord, C. J. & Ashworth, A. PARP inhibitors: synthetic lethality in the clinic. *Science* **355**, 1152–1158 (2017).
36. Galluzzi, L. *et al.* Systems biology of cisplatin resistance: past, present and future. *Cell Death Dis.* **5**, e1257 (2014).
37. Easwaran, H., Tsai, H. C. & Baylin, S. B. Cancer epigenetics: tumor heterogeneity, plasticity of stem-like states, and drug resistance. *Mol. Cell* **54**, 716–727 (2014).
38. Galluzzi, L. *et al.* Consensus guidelines for the definition, detection and interpretation of immunogenic cell death. *J. Immunother. Cancer* **8**, e000337 (2020).

39. Vasan, N., Baselga, J. & Hyman, D. M. A view on drug resistance in cancer. *Nature* **575**, 299–309 (2019).
40. Rottenberg, S. *et al.* High sensitivity of BRCA1-deficient mammary tumors to the PARP inhibitor AZD2281 alone and in combination with platinum drugs. *Proc. Natl Acad. Sci. USA* **105**, 17079–17084 (2008).
41. Dai, Y. *et al.* Correction: involvement of Bcl-2 family proteins in AKT-regulated cell survival in cisplatin-resistant epithelial ovarian cancer. *Oncotarget* **11**, 488–489 (2020).
42. Denoyer, D. *et al.* Targeting copper in cancer therapy: "copper that cancer". *Metallomics* **7**, 1459–1476 (2015).
43. Yuan, X. *et al.* Notch signaling: an emerging therapeutic target for cancer treatment. *Cancer Lett.* **369**, 20–27 (2015).
44. Wang, Z. *et al.* Targeting Notch signaling pathway to overcome drug resistance for cancer therapy. *Biochim. Biophys. Acta* **1806**, 258–267 (2010).
45. Liu, J. *et al.* NOTCH1 regulates DNA damage response and sorafenib resistance by activating ATM in hepatocellular carcinoma. *Am. J. Transl. Res.* **16**, 7317–7329 (2024).
46. Chen, Z. X. *et al.* Hypoxia-induced DTL promotes proliferation, metastasis, and sorafenib resistance of hepatocellular carcinoma via ubiquitin-mediated degradation of SLTM and activation of Notch signaling. *Cell Death Dis.* **15**, 734 (2024).
47. Adamowicz, M., Vermezovic, J. & d'Adda di Fagagna, F. NOTCH1 inhibits activation of ATM by impairing formation of an ATM–FOXO3a–KAT5/Tip60 complex. *Cell Rep.* **16**, 2068–2076 (2016).
48. Tong, X. *et al.* Targeting cell death pathways for cancer therapy: recent developments in necroptosis, pyroptosis, ferroptosis, and cuproptosis. *J. Hematol. Oncol.* **15**, 174 (2022).

Figure and table legends

Figure 1. *ATOX1* is identified as a key regulatory gene for cisplatin resistance in liver cancer.

(A) Schematic diagram of CRISPR-Cas9 gene screen model in HepG2 and Huh7 liver cancer cell

lines. (B-C) sgRNA number distribution of HepG2 and Huh7 cells on day 0. (D) KEGG pathway analysis of cisplatin resistance genes in HepG2 cells. (E) KEGG pathway analysis of cisplatin resistance genes in Huh7 cells. (F) 67 cisplatin resistance genes shared common between HepG2 and Huh7 cells. (G) Z-score plots indicated the cisplatin resistance genes with top10 drugZ score in two liver cancer cell lines. (H) Changes of targeting *ATOX1* sgRNAs in two liver cancer cell lines in day0, DMSO and cisplatin treatment group. (I) Expression of ATOX1 protein was detected in human immortalized hepatocyte cell line THLE-2 and various liver cancer cell lines, including HepG2, Huh1, Hep3B, SNU449, JHH7, Huh7, Li-7, and SNU-475 (n = 3). (J) CCK-8 was used to detect the IC50 of cisplatin in liver cancer cell lines (n =3). (K) Liver cancer cell lines with high ATOX1 protein expression exhibited high IC50 of cisplatin. **P < 0.01.

Figure 2. High expression of ATOX1 is significantly associated with poor prognosis and cisplatin resistance in liver cancer patients. (A) Immunohistochemical staining of ATOX1 in liver cancer tissues and adjacent tissues (n = 60). Black bar means 100 μm. (B) Quantitative analysis of ATOX1 expression levels in liver cancer tissues and adjacent tissues (n = 60). (C) Comparison of ATOX1 expression in paired liver cancer tissues and adjacent tissues (n = 60). (D) ROC curve of ATOX1 as a discriminator of liver cancer disease status. (E) ROC curve of ATOX1 for predicting recurrence risk. (F) Relationship between ATOX1 expression and overall survival. (G) Relationship between ATOX1 expression and disease-free survival. (H) Nomogram model incorporating ATOX1 expression for predicting liver cancer patient survival. (I) Comparison of cisplatin resistance scores between high and low *ATOX1* expression groups in TCGA and ICGC datasets. (J) Correlation analysis between *ATOX1* expression and cisplatin resistance scores in TCGA and ICGC datasets. n=369 (TCGA), n=243 (ICGC). **, P < 0.01.

Fig. 3. ATOX1 reduced the sensitivity of liver cancer cells to cisplatin. (A) qRT-PCR results indicated that the si1-*ATOX1* exhibited the significant effects on reducing the mRNA levels of *ATOX1* (n = 3). (B) Western blotting results indicated that the si1-ATOX1 exhibited the significant

effects on reducing the protein levels of ATOX1 (n = 3). (C) CCK-8 assay was used to detect the IC50 of cisplatin in NC and *ATOX1*-knockdown liver cancer cells (n = 3). (D-E) qRT-PCR and western blotting results indicated that ATOX1-overexpressing HepG2 and Huh7 cells were constructed (n = 3). (F) CCK-8 assay was used to detect the IC50 of cisplatin in vector and *ATOX1*-overexpressing liver cancer cells (n = 3). (G) EdU staining showing cell proliferation in different treatment groups including NC+DMSO, si-*ATOX1*+DMSO, NC+cisplatin, and si-*ATOX1*+cisplatin (n = 3). White bar means 100 μm. (H) Colony formation assay evaluating the long-term proliferation capacity of liver cancer cells in NC+DMSO, si-*ATOX1*+DMSO, NC+cisplatin, and si-*ATOX1*+cisplatin groups (n = 3). (I) Flow cytometry analysis of apoptosis rates in different treatment groups including NC+DMSO, si-*ATOX1*+DMSO, NC+cisplatin, and si-*ATOX1*+cisplatin (n = 3). (J-L) Tumor growth in the groups including NC+DMSO, sh-*ATOX1*+DMSO, NC+cisplatin, and sh-*ATOX1*+cisplatin (n = 5/group). (M) Tumor weight in the groups including NC+DMSO, sh-*ATOX1*+DMSO, NC+cisplatin, and sh-*ATOX1*+cisplatin (n = 5/group). (N) IHC results of ATOX1 and KI67 expression in NC+DMSO, sh-*ATOX1*+DMSO, NC+cisplatin, and sh-*ATOX1*+cisplatin groups (n = 5/group). Black bar means 100 μm.**, $P < 0.01$.

Figure 4. Compound 8 identified as an efficient ATOX1-specific inhibitor with excellent binding affinity and pharmacokinetic properties. (A) Conformational changes of ATOX1 protein at 0ns, 50ns, and 100ns time points. (B) RMSD value fluctuation of ATOX1 protein in molecular dynamics simulation. (C) Residue fluctuation analysis (RMSF) results of ATOX1 protein. (D) Virtual screening process based on ChemDiv database. (E) Chemical structures of representative lead compounds, as well as positive drugs DC_AC50. (F) Fluorescence spectral analysis (FRET) results of compound 8 and DC_AC50. (G) FRET experimental verification results of compound 8 and its 9 analogues. (H) Surface plasmon resonance analysis showing binding affinity of compound 8 to ATOX1 protein. (I) PTS experiments revealed signal intensity of compound 8 at different concentrations. (J) Analysis of key interaction sites between compound 8

and ATOX1 protein. (K) Molecular dynamics simulations showed that the 8/ATOX1 complex exhibited high conformational stability. (L) Residue contribution analysis for the 8/ATOX1 complex. (M) Binding free energy analysis for the 8/ATOX1 complex. (N) ADMET analysis indicated that compound 8 performed well in terms of blood-brain barrier permeability.

Figure 5. ATOX1 inhibitor demonstrates significant synergistic anti-tumor effects with cisplatin on liver cancer cell. (A) Cell survival curves and IC50 values of compound 8 and DC_AC50 on THLE-2, HepG2 and Huh7 when used alone (n = 3). (B-C) Heat map demonstrated the synergistic effects at different concentration combinations (n = 3). (D) EDU positive rate in DMSO, compound 8, cisplatin and combine treatment group (n = 3). White bar means 100 μm. (E) Colony formation assay showing clonogenic ability in DMSO, compound 8, cisplatin and combine treatment group (n = 3). (F) Annexin V/PI double staining flow cytometry analysis of apoptosis rates in DMSO, compound 8, cisplatin and combine treatment group (n = 3). (G) Research design of HepG2 liver cancer cell xenograft model. (H) Tumor volume growth curves of DMSO, compound 8, cisplatin and combine treatment group (n = 5/group). (I) *In vivo* imaging results of DMSO, compound 8, cisplatin and combine treatment group (n = 5/group). (J) Comparison of tumor tissues from each group after experiment completion (n = 5/group). (K) Immunohistochemical analysis results and scores of KI67 and PCNA (n = 5/group). White bar means 100 μm. (L) HE staining results of major organs (heart, liver, gastrointestinal tract, lung, kidney) from each treatment group (n = 5/group). Black bar means 100 μm.**, $P<0.01$.

Figure 6. Targeted inhibition of ATOX1 by compound 8 increases DNA methylation at the *NOTCH1* promoter in a copper-dependent manner. (A) Principal component analysis revealed distinct clustering patterns among the treatment group. (B) DEGs analysis for compound 8, cisplatin and combine treatment compared with DMSO treatment group. (C) KEGG pathway enrichment analysis of the DEGs regulated by compound 8. (D) GSEA analysis of NOTCH signaling for the gene changes induced by compound 8, cisplatin and their combination. (E)

mRNA levels of *NOTCH1* and *HES1* in liver cancer cells in the NC and *ATOX1* knockdown groups (n =3). (F) Protein levels of NOTCH1 and HES1 in liver cancer cells in the NC and ATOX1 knockdown groups (n =3). (G) qRT-PCR was used to detect the effects of compound 8 on the mRNA levels of *NOTCH1* and *HES1* (n =3). (H) Western blotting was used to detect the effects of compound 8 on the protein levels of NOTCH1 and HES1 (n =3). (I) Immunofluorescence staining showed that treatment with compound 8 significantly reduced both the overall expression and nuclear localization of NOTCH1 protein in liver cancer cells (n =3). White bar means 100 μm. (J-K) TTM treatment significantly alleviated the *ATOX1* knockdown–induced reduction in NOTCH1 and HES1 expression at both the mRNA and protein levels (n =3). (L) TTM markedly attenuated the hypermethylation induced by *ATOX1* depletion (n =3). (M) Compound 8 increased intracellular copper levels in liver cancer cells (n =3). (N) Compound 8 increased DNA methylation within the *NOTCH1* promoter region in liver cancer cells (n =3). (O) TTM treatment significantly suppressed compound 8–induced *NOTCH1* promoter methylation (n =3). (P-Q) qRT-PCR and western blotting analysis indicated that TTM treatment significantly reduced transcriptional and protein-level repression of NOTCH1 and HES1 induced by compound 8 (n =3). *, $P<0.05$; **, $P<0.01$.

Figure 7. The synergistic effect between compound 8 and cisplatin is dependent on the ATOX1/NOTCH1 axis. (A) The effects of compound 8 on methylation level of the NOTCH1 promoter in liver cancer cells with ATOX1 knockdown (n =3). (B) The effects of compound 8 on mRNA levels of *NOTCH1* and *HES1* in liver cancer cells with ATOX1 knockdown (n =3). (C) Western blotting analysis indicated the effects of compound 8, cisplatin and combination on the expression of NOTCH1 and HES1 in NC and si-*ATOX1* cells (n =3). (D) Colony formation assay analyzed the effects of compound 8, cisplatin and combination on liver cancer cells with *ATOX1*-knockdown (n =3). (E) The EdU incorporation assay analyzed the effects of compound 8, cisplatin and combination on liver cancer cells with *ATOX1*-knockdown (n =3). White bar means 100 μm. (F) *NOTCH1* overexpressing liver cancer cells were constructing (n =3). (G) CCK-8 assays

indicated that the combination of compound 8 and cisplatin exhibited weaker inhibitory effects on liver cancer cells with *NOTCH1*-overexpression (n =3). (H) EdU assays indicated that the combination of compound 8 and cisplatin exhibited weaker inhibitory effects on liver cancer cells with *NOTCH1*-overexpression (n =3). White bar means 50 μm. Ns, no significant; **, P<0.01.

Table 1. Results of compound screening.

Table 2. Structural analogs of Compound 8 with similarity scores exceeding 90%.

Table 1. Results of compound screening

ID	Chemical structure	Docking Score (kcal/mol)	Recover (%)	Remarks
5593-1988	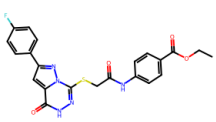	-13.283	<60%	
D315-1941	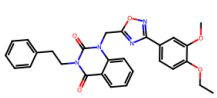	-13.060	<60%	
D315-1867	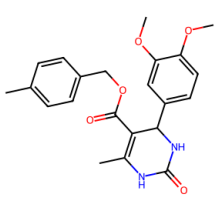	-13.032	<60%	

8019-3658	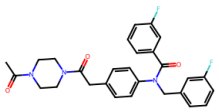	-13.003	<60%	
V027-7833	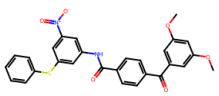	-12.811	<60%	
V019-4692	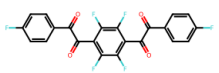	-12.751	<60%	
V016-7804	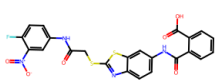	-12.604	<60%	
Y041-1442	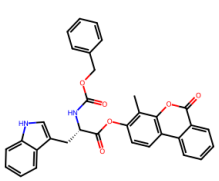	-12.589	**95%**	**8#**
J059-0200	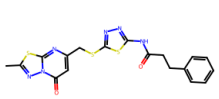	-12.527	<60%	

Y070-3936	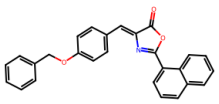	-12.338	<60%
8017-2987	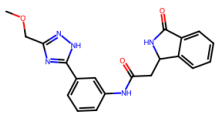	-12.276	<60%
4489-7858	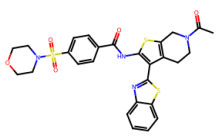	-12.240	<60%
Y041-8961	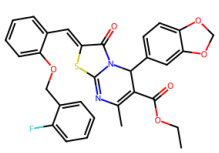	-12.219	<60%
Y041-2399	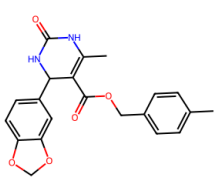	-12.211	<60%
L110-0432	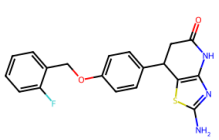	-12.186	<60%

3999-6353	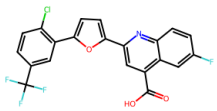	-12.181	<60%	
4099-6456	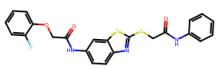	-12.177	<60%	
T226-2130	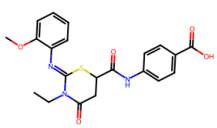	-12.069	<60%	
L453-0494	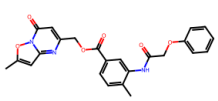	-12.044	<60%	
D300-0307	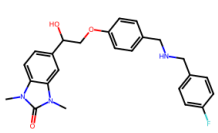	-11.918	**89%**	**29#**
K408-0891	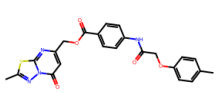	-11.873	<60%	

E734-2555	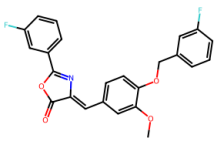	-11.865	<60%
G856-8744	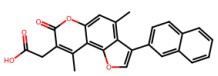	-11.822	<60%
G357-4720	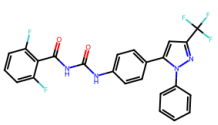	-11.688	<60%
8007-2260	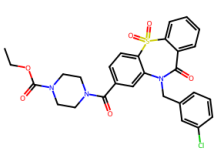	-11.681	<60%
D481-0111	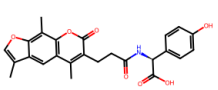	-11.671	<60%
L707-0418	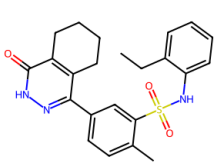	-11.573	<60%

5775-2709	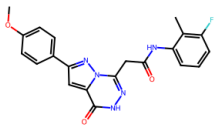	-11.556	<60%	
L681-0284	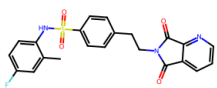	-11.489	<60%	
5201-0104	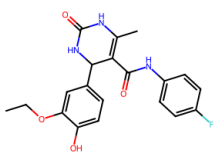	-11.440	**93%**	**25#**
D585-0146	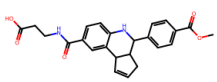	-11.359	<60%	
P671-2205	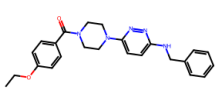	-11.335	<60%	
E772-0278	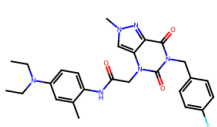	-11.306	<60%	

D074-0524	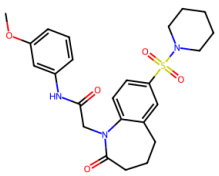	-11.216	<60%
8013-1039	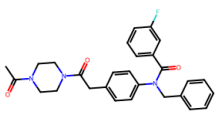	-11.215	<60%
C597-0263	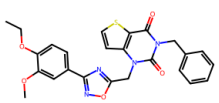	-11.203	<60%
3270-0609	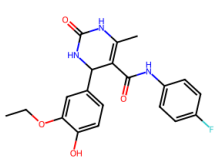	-11.146	<60%
F455-0480	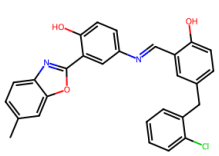	-11.104	<60%
1037-1152	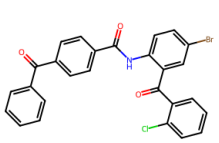	-11.073	<60%

G807-0587	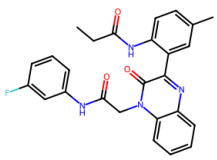	-11.021	<60%
G545-0293	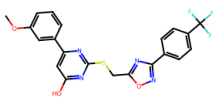	-10.986	<60%
D336-1878	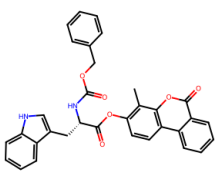	-10.968	<60%
D151-0474	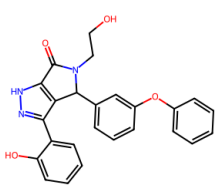	-10.946	<60%
2154-0616	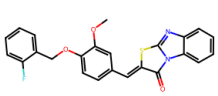	-10.932	<60%
L927-0251	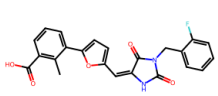	-10.832	<60%

8009-2929	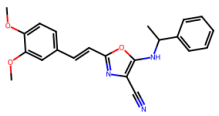	-10.741	<60%
2044-1708	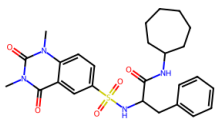	-10.725	<60%
E903-0649	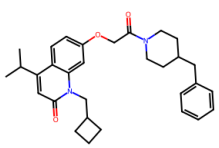	-10.672	<60%
F424-0152	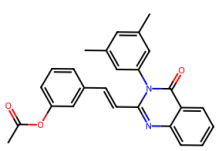	-10.632	<60%
3970-1841	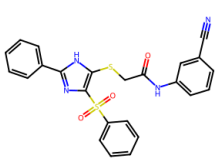	-10.601	<60%
C679-6580	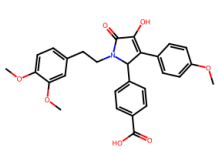	-10.582	<60%

Y500-5028	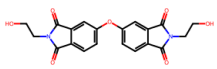	-10.578	<60%
G357-0031	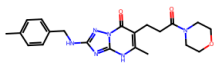	-10.537	<60%
D298-0206	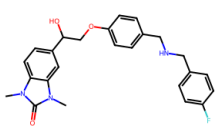	-10.521	<60%
2062-1075	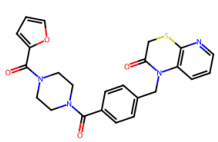	-10.497	<60%
K788-8635	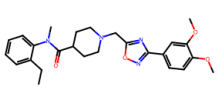	-10.497	<60%
G072-1899	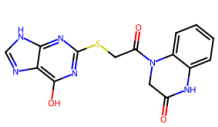	-10.368	<60%

D050-0132	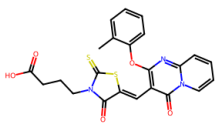	-10.344	<60%	
8009-1862	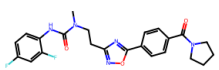	-10.313	<60%	
D129-0133	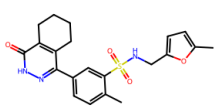	-10.226	<60%	
K505-0870	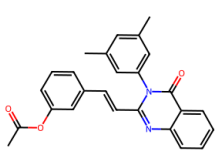	-10.120	**78%**	**52#**
8016-6378	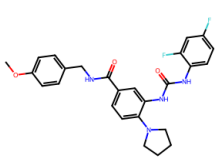	-9.940	<60%	
8016-0967	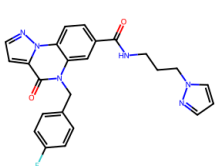	-9.477	<60%	

Table 2. Structural analogs of Compound 8 with similarity scores exceeding 90%.

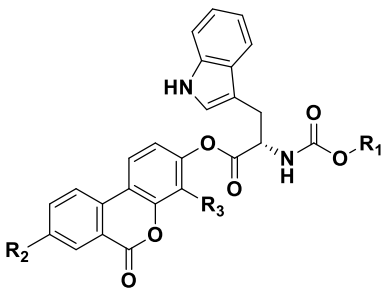

compound	R1	R2	R3
STL461817		H	CH_3
STL462726	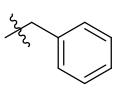		H
STL461809	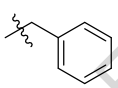		CH_3

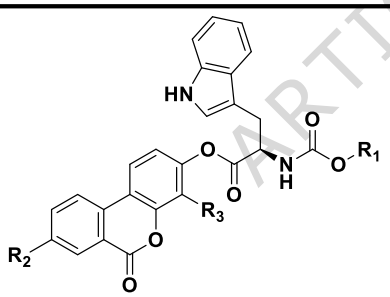

compound	R1	R2	R3
STK024854	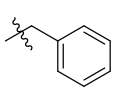	H	H
STL529841			CH_3

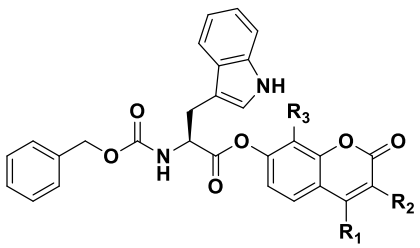

compound	R1	R2	R3
STL528695	CH_3	CH_3	H
STL462307		H	CH_3

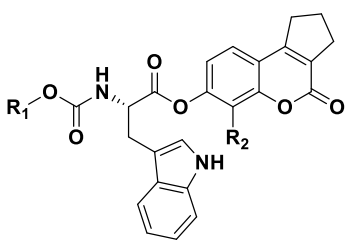

compound	R1	R2
STL461777		H
STL529234	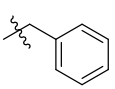	CH_3

Editorial summary:

ATOX1 inhibitor Compound 8 increases NOTCH1 promoter methylation, suppresses NOTCH1/HES1 signaling, and sensitizes liver cancer cells to cisplatin.

Peer review information:
Communications Biology thanks the anonymous reviewers for their contribution to the peer review of this work. Primary Handling Editors: Joanna Timmins and Mengtan Xing. A peer review file is available.

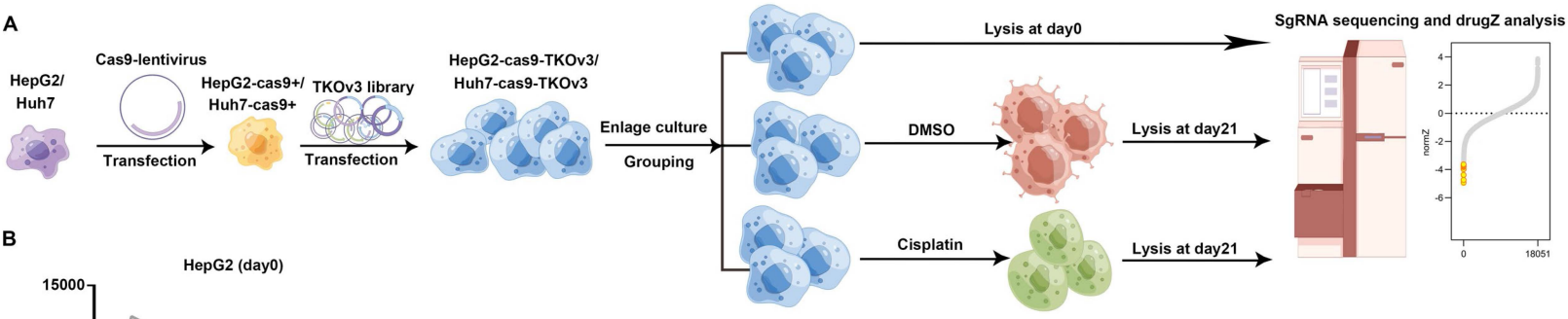
A
HepG2/
Huh7
Cas9-lentivirus
Transfection
HepG2-cas9+/
Huh7-cas9+
TKOv3 library
Transfection
HepG2-cas9-TKOv3/
Huh7-cas9-TKOv3
Enlage culture
Grouping
Lysis at day0
DMSO
Lysis at day21
Cisplatin
Lysis at day21
SgRNA sequencing and drugZ analysis
normZ

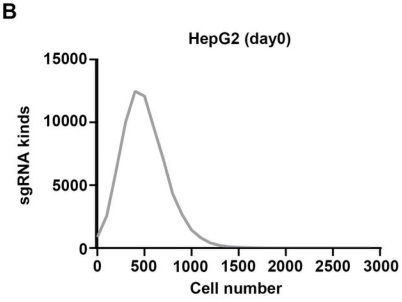
B
HepG2 (day0)
sgRNA kinds
Cell number

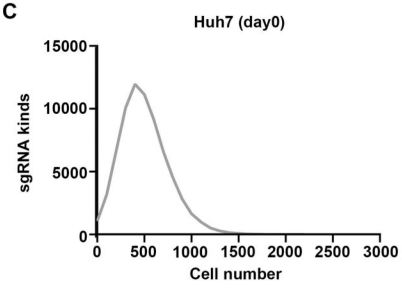
C
Huh7 (day0)
sgRNA kinds
Cell number

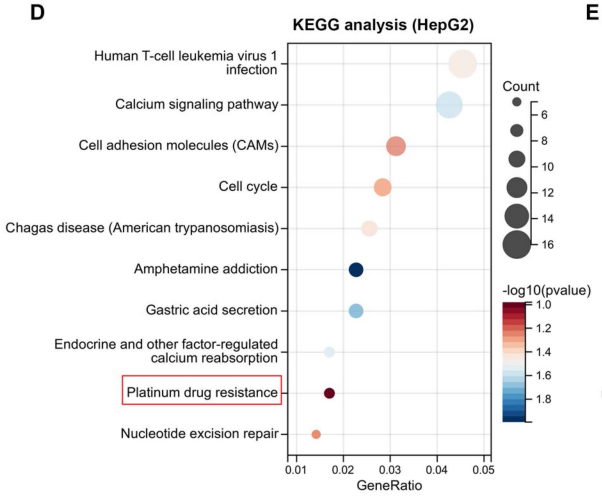
D
KEGG analysis (HepG2)
Human T-cell leukemia virus 1 infection
Calcium signaling pathway
Cell adhesion molecules (CAMs)
Cell cycle
Chagas disease (American trypanosomiasis)
Amphetamine addiction
Gastric acid secretion
Endocrine and other factor-regulated calcium reabsorption
Platinum drug resistance
Nucleotide excision repair
Count
-log10(pvalue)
GeneRatio

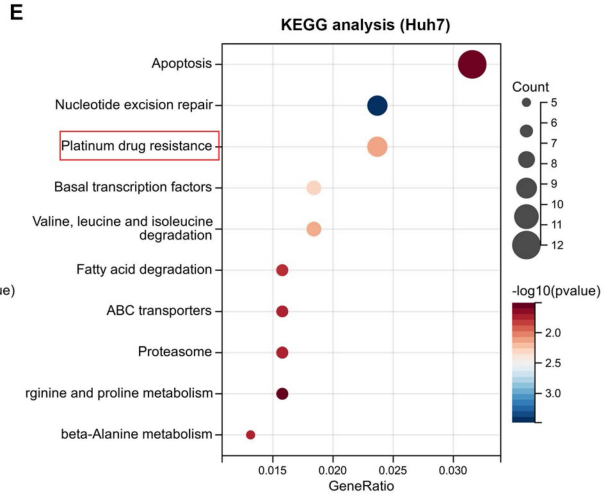
E
KEGG analysis (Huh7)
Apoptosis
Nucleotide excision repair
Platinum drug resistance
Basal transcription factors
Valine, leucine and isoleucine degradation
Fatty acid degradation
ABC transporters
Proteasome
rginine and proline metabolism
beta-Alanine metabolism
Count
-log10(pvalue)
GeneRatio

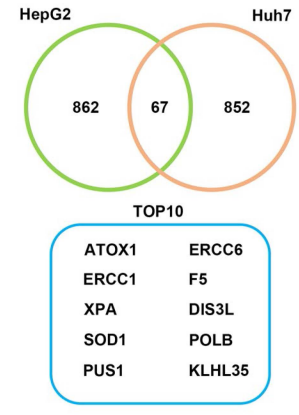
F
HepG2
Huh7
862
67
852
TOP10
ATOX1
ERCC1
XPA
SOD1
PUS1
ERCC6
F5
DIS3L
POLB
KLHL35

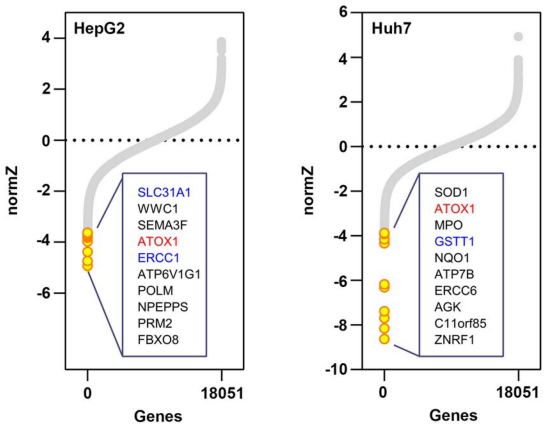
G
HepG2
normZ
SLC31A1
WWC1
SEMA3F
ATOX1
ERCC1
ATP6V1G1
POLM
NPEPPS
PRM2
FBXO8
Genes
Huh7
normZ
SOD1
ATOX1
MPO
GSTT1
NQO1
ATP7B
ERCC6
AGK
C11orf85
ZNRF1
Genes

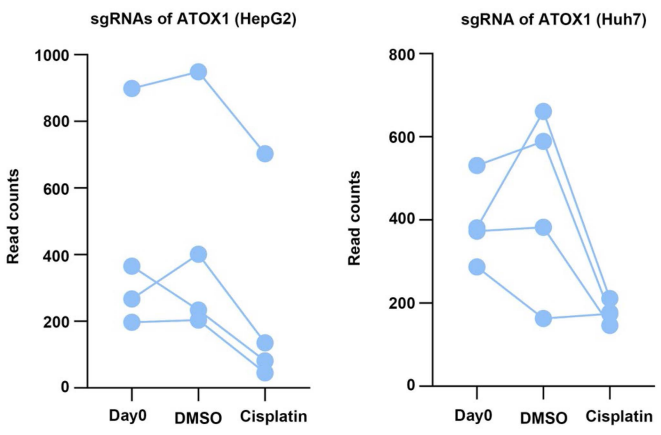
H
sgRNAs of ATOX1 (HepG2)
Read counts
Day0
DMSO
Cisplatin
sgRNA of ATOX1 (Huh7)
Read counts
Day0
DMSO
Cisplatin

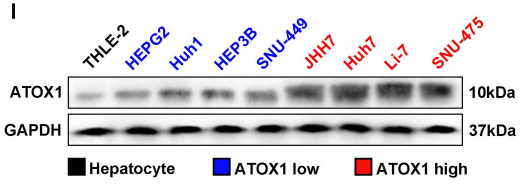
I
THLE-2
HEPG2
Huh1
HEP3B
SNU-449
JHH7
Huh7
Li-7
SNU-475
ATOX1
10kDa
GAPDH
37kDa
Hepatocyte
ATOX1 low
ATOX1 high

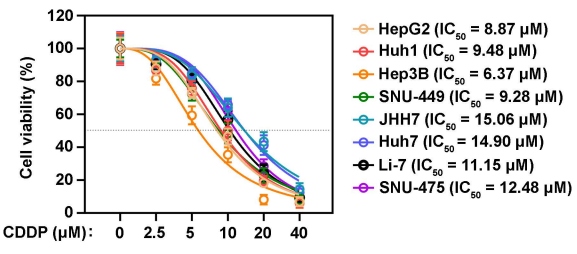
J
Cell viability (%)
CDDP (μM): 0 2.5 5 10 20 40
HepG2 (IC50 = 8.87 μM)
Huh1 (IC50 = 9.48 μM)
Hep3B (IC50 = 6.37 μM)
SNU-449 (IC50 = 9.28 μM)
JHH7 (IC50 = 15.06 μM)
Huh7 (IC50 = 14.90 μM)
Li-7 (IC50 = 11.15 μM)
SNU-475 (IC50 = 12.48 μM)

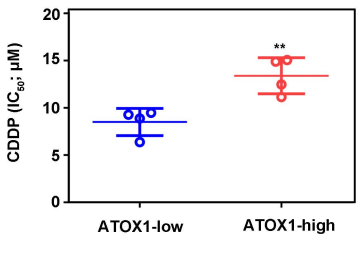
K
CDDP (IC50; μM)
**
ATOX1-low
ATOX1-high

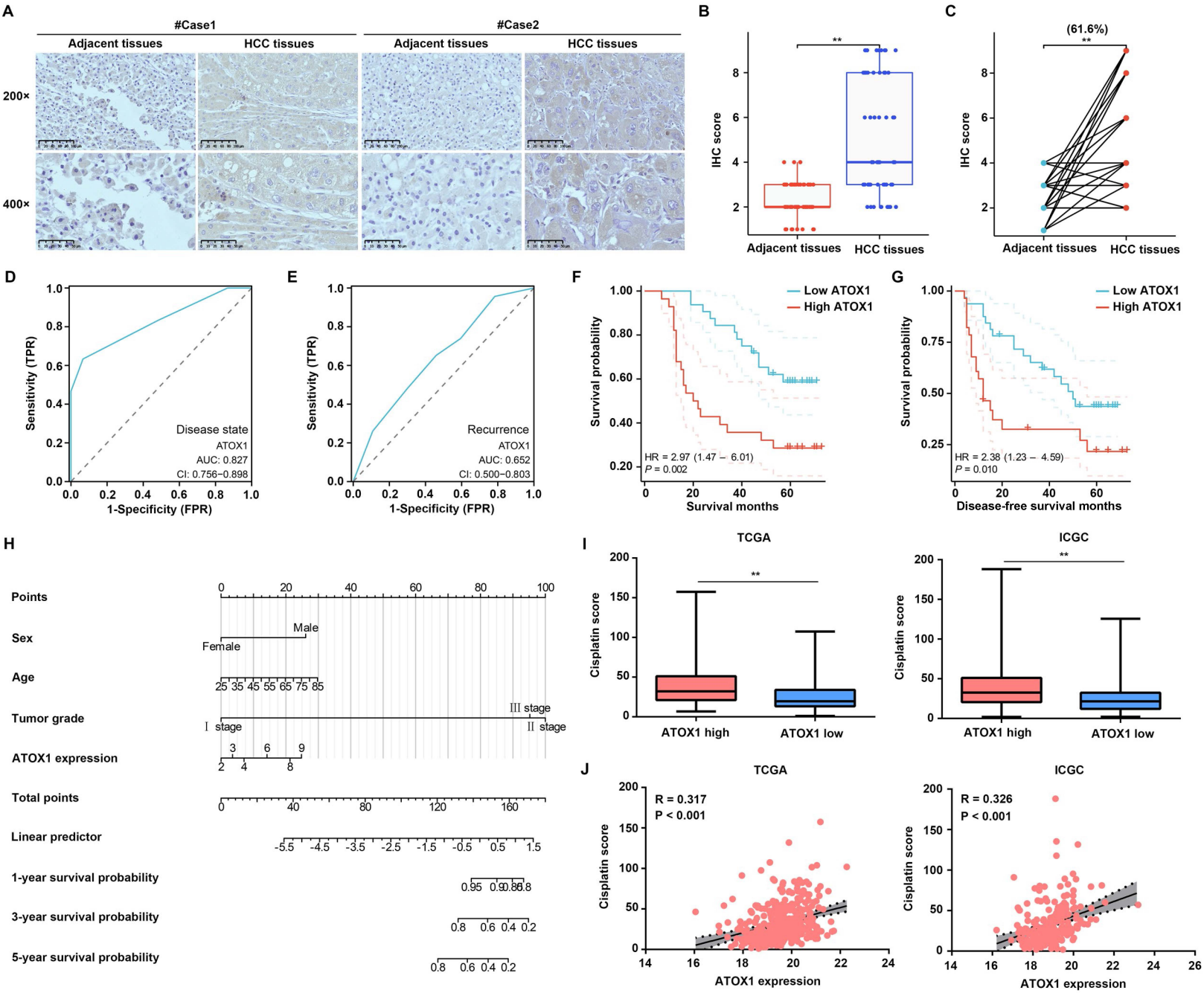
A
#Case1
#Case2
Adjacent tissues
HCC tissues
Adjacent tissues
HCC tissues
200×
400×
B
IHC score
**
Adjacent tissues
HCC tissues
C
(61.6%)
**
IHC score
Adjacent tissues
HCC tissues
D
Sensitivity (TPR)
1-Specificity (FPR)
Disease state
ATOX1
AUC: 0.827
CI: 0.756−0.898
E
Sensitivity (TPR)
1-Specificity (FPR)
Recurrence
ATOX1
AUC: 0.652
CI: 0.500−0.803
F
Low ATOX1
High ATOX1
Survival probability
HR = 2.97 (1.47 − 6.01)
P = 0.002
Survival months
G
Low ATOX1
High ATOX1
Survival probability
HR = 2.38 (1.23 − 4.59)
P = 0.010
Disease-free survival months
H
Points
Sex
Male
Female
Age
25 35 45 55 65 75 85
Tumor grade
III stage
I stage
II stage
ATOX1 expression
3 6 9
2 4 8
Total points
Linear predictor
1-year survival probability
3-year survival probability
5-year survival probability
I
TCGA
ICGC
Cisplatin score
**
ATOX1 high
ATOX1 low
J
TCGA
ICGC
R = 0.317
P < 0.001
R = 0.326
P < 0.001
Cisplatin score
ATOX1 expression

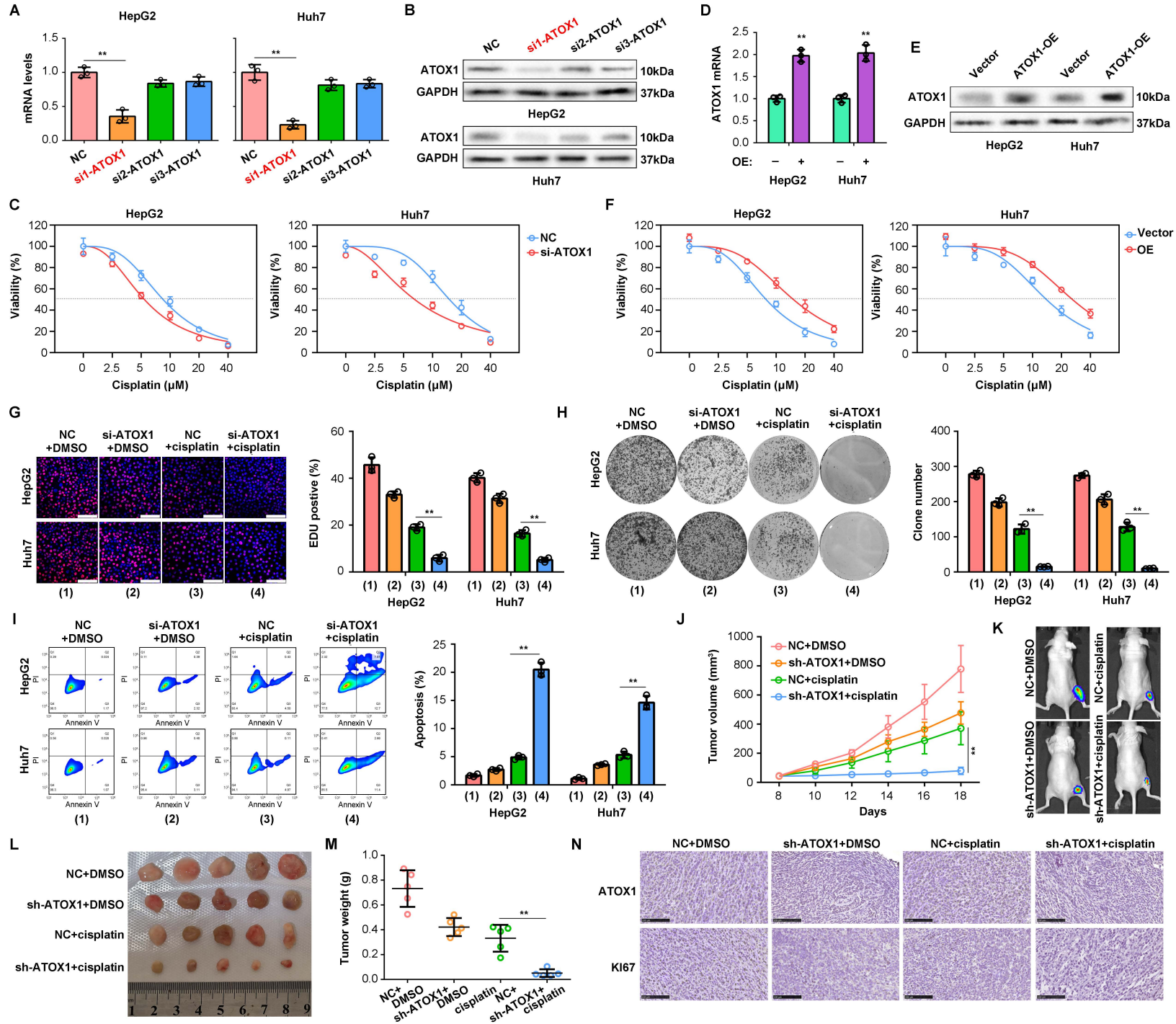
A
HepG2
Huh7
mRNA levels
NC
si1-ATOX1
si2-ATOX1
si3-ATOX1
B
ATOX1
GAPDH
10kDa
37kDa
D
ATOX1 mRNA
OE:
E
Vector
ATOX1-OE
C
Viability (%)
Cisplatin (μM)
F
G
EDU postive (%)
H
Clone number
I
Annexin V
PI
Apoptosis (%)
J
Tumor volume (mm³)
Days
K
L
M
Tumor weight (g)
N
KI67

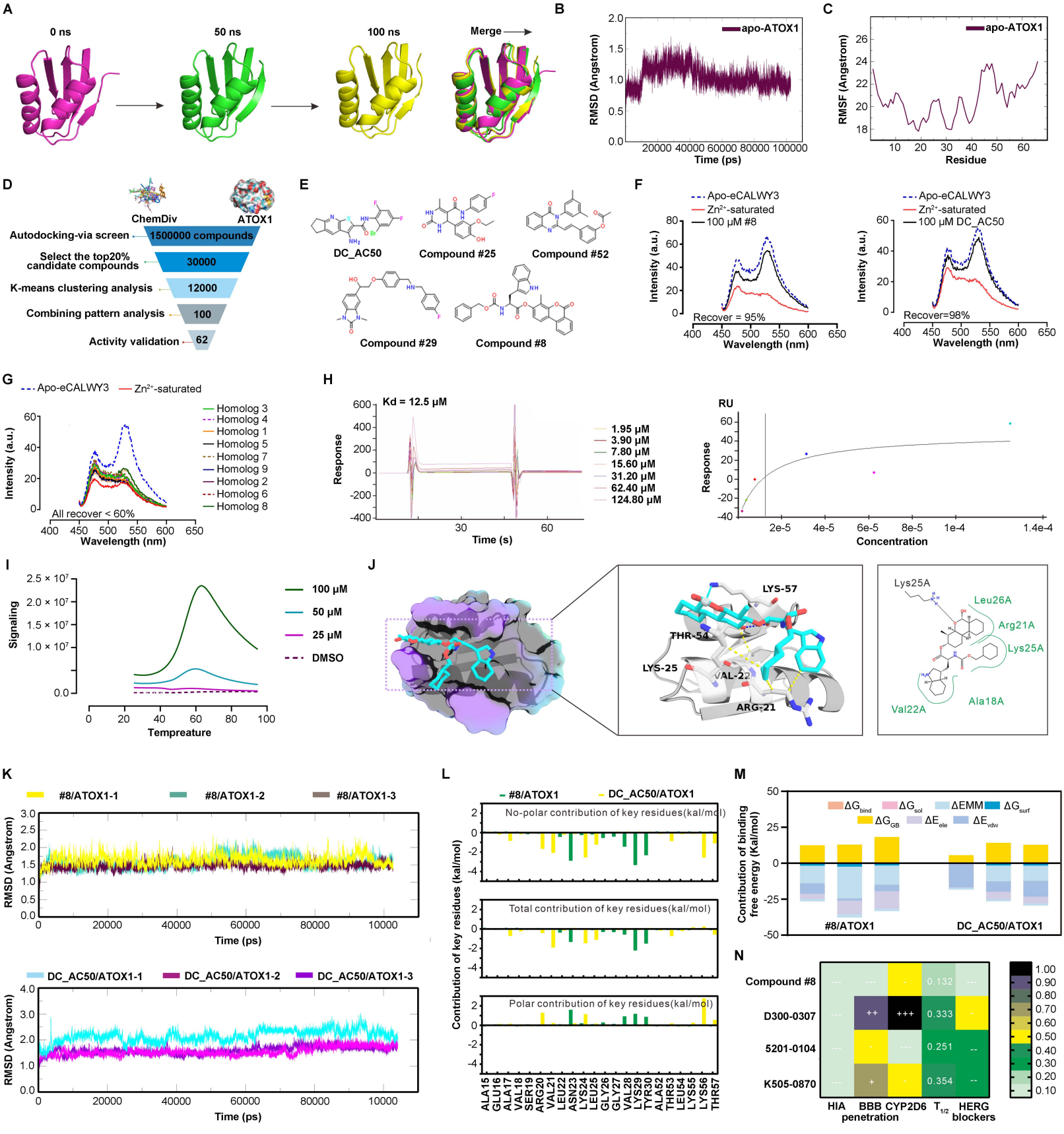
A
0 ns
50 ns
100 ns
Merge
B
apo-ATOX1
RMSD (Angstrom)
Time (ps)
C
apo-ATOX1
RMSF (Angstrom)
Residue
D
ChemDiv
ATOX1
Autodocking-via screen
1500000 compounds
Select the top20% candidate compounds
30000
K-means clustering analysis
12000
Combining pattern analysis
100
Activity validation
62
E
DC_AC50
Compound #25
Compound #52
Compound #29
Compound #8
F
Apo-eCALWY3
Zn²⁺-saturated
100 μM #8
Recover = 95%
100 μM DC_AC50
Recover=98%
Intensity (a.u.)
Wavelength (nm)
G
Apo-eCALWY3
Zn²⁺-saturated
Homolog 3
Homolog 4
Homolog 1
Homolog 5
Homolog 7
Homolog 9
Homolog 2
Homolog 6
Homolog 8
All recover < 60%
H
Kd = 12.5 μM
1.95 μM
3.90 μM
7.80 μM
15.60 μM
31.20 μM
62.40 μM
124.80 μM
Response
Time (s)
RU
Concentration
I
Signaling
100 μM
50 μM
25 μM
DMSO
Tempreature
J
LYS-57
THR-54
LYS-25
VAL-22
ARG-21
Lys25A
Leu26A
Arg21A
Lys25A
Ala18A
Val22A
K
#8/ATOX1-1
#8/ATOX1-2
#8/ATOX1-3
RMSD (Angstrom)
Time (ps)
DC_AC50/ATOX1-1
DC_AC50/ATOX1-2
DC_AC50/ATOX1-3
L
#8/ATOX1
DC_AC50/ATOX1
No-polar contribution of key residues(kal/mol)
Total contribution of key residues(kal/mol)
Polar contribution of key residues(kal/mol)
Contribution of key residues (kal/mol)
ALA15 GLU16 ALA17 VAL18 SER19 ARG20 VAL21 LEU22 ASN23 LYS24 LEU25 GLY26 GLY27 VAL28 LYS29 TYR30 ALA52 THR53 LEU54 LYS55 LYS56 THR57
M
ΔG_bind
ΔG_sol
ΔEMM
ΔG_surf
ΔG_GB
ΔE_ele
ΔE_vdw
Contribution of binding free energy (Kal/mol)
#8/ATOX1
DC_AC50/ATOX1
N
Compound #8
D300-0307
5201-0104
K505-0870
0.132
0.333
0.251
0.354
HIA
BBB penetration
CYP2D6
T1/2
HERG blockers

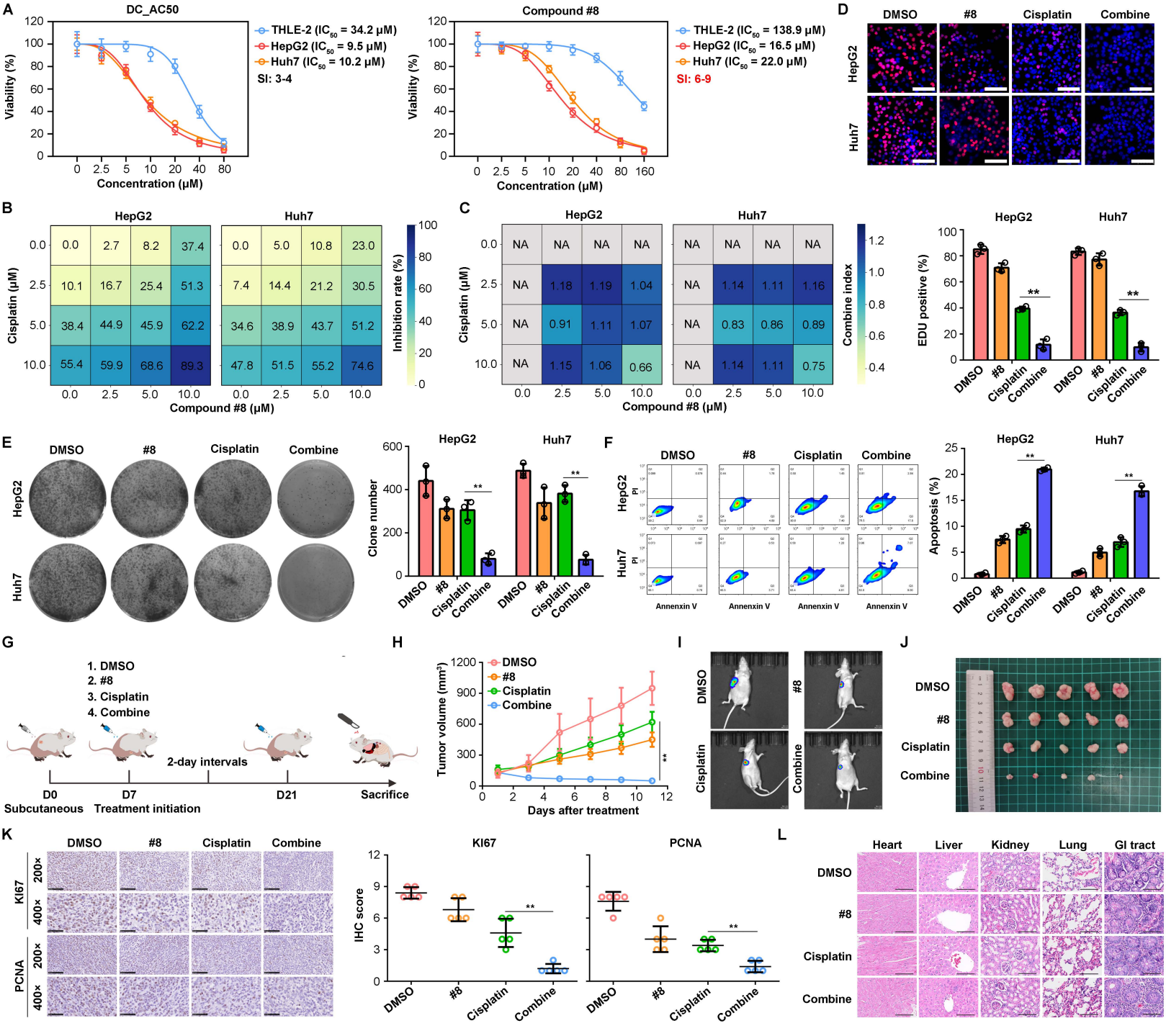
A
DC_AC50
Viability (%)
Concentration (μM)
THLE-2 (IC50 = 34.2 μM)
HepG2 (IC50 = 9.5 μM)
Huh7 (IC50 = 10.2 μM)
SI: 3-4
Compound #8
THLE-2 (IC50 = 138.9 μM)
HepG2 (IC50 = 16.5 μM)
Huh7 (IC50 = 22.0 μM)
SI: 6-9
B
HepG2
Huh7
Cisplatin (μM)
Compound #8 (μM)
Inhibition rate (%)
C
Combine index
D
DMSO
#8
Cisplatin
Combine
EDU positive (%)
E
Clone number
F
PI
Annexin V
Apoptosis (%)
G
1. DMSO
2. #8
3. Cisplatin
4. Combine
2-day intervals
D0
D7
D21
Sacrifice
Subcutaneous
Treatment initiation
H
Tumor volume (mm³)
Days after treatment
I
J
K
KI67
PCNA
IHC score
L
Heart
Liver
Kidney
Lung
GI tract

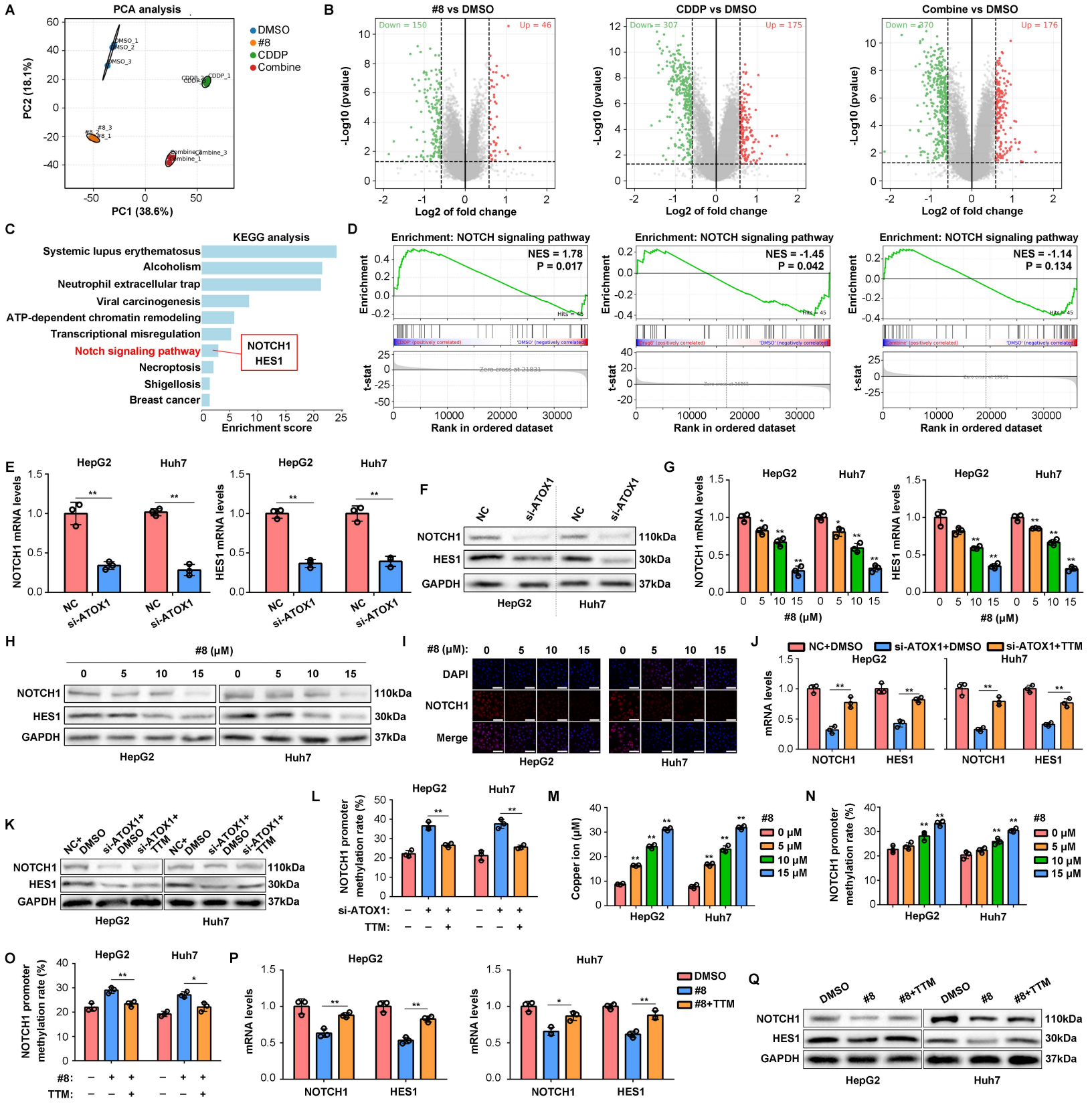
A
PCA analysis
DMSO
#8
CDDP
Combine
PC1 (38.6%)
PC2 (18.1%)
B
#8 vs DMSO
CDDP vs DMSO
Combine vs DMSO
Down = 150
Up = 46
Down = 307
Up = 175
Down = 370
Up = 176
-Log10 (pvalue)
Log2 of fold change
C
KEGG analysis
Systemic lupus erythematosus
Alcoholism
Neutrophil extracellular trap
Viral carcinogenesis
ATP-dependent chromatin remodeling
Transcriptional misregulation
Notch signaling pathway
Necroptosis
Shigellosis
Breast cancer
NOTCH1
HES1
Enrichment score
D
Enrichment: NOTCH signaling pathway
NES = 1.78
P = 0.017
NES = -1.45
P = 0.042
NES = -1.14
P = 0.134
Enrichment
t-stat
Rank in ordered dataset
E
HepG2
Huh7
NOTCH1 mRNA levels
HES1 mRNA levels
NC
si-ATOX1
F
NOTCH1
HES1
GAPDH
110kDa
30kDa
37kDa
G
#8 (μM)
H
#8 (μM)
I
DAPI
NOTCH1
Merge
J
NC+DMSO
si-ATOX1+DMSO
si-ATOX1+TTM
mRNA levels
K
NC+ DMSO
si-ATOX1+ DMSO
si-ATOX1+ TTM
L
NOTCH1 promoter methylation rate (%)
si-ATOX1:
TTM:
M
Copper ion (μM)
#8
0 μM
5 μM
10 μM
15 μM
N
O
#8:
P
DMSO
#8
#8+TTM
Q

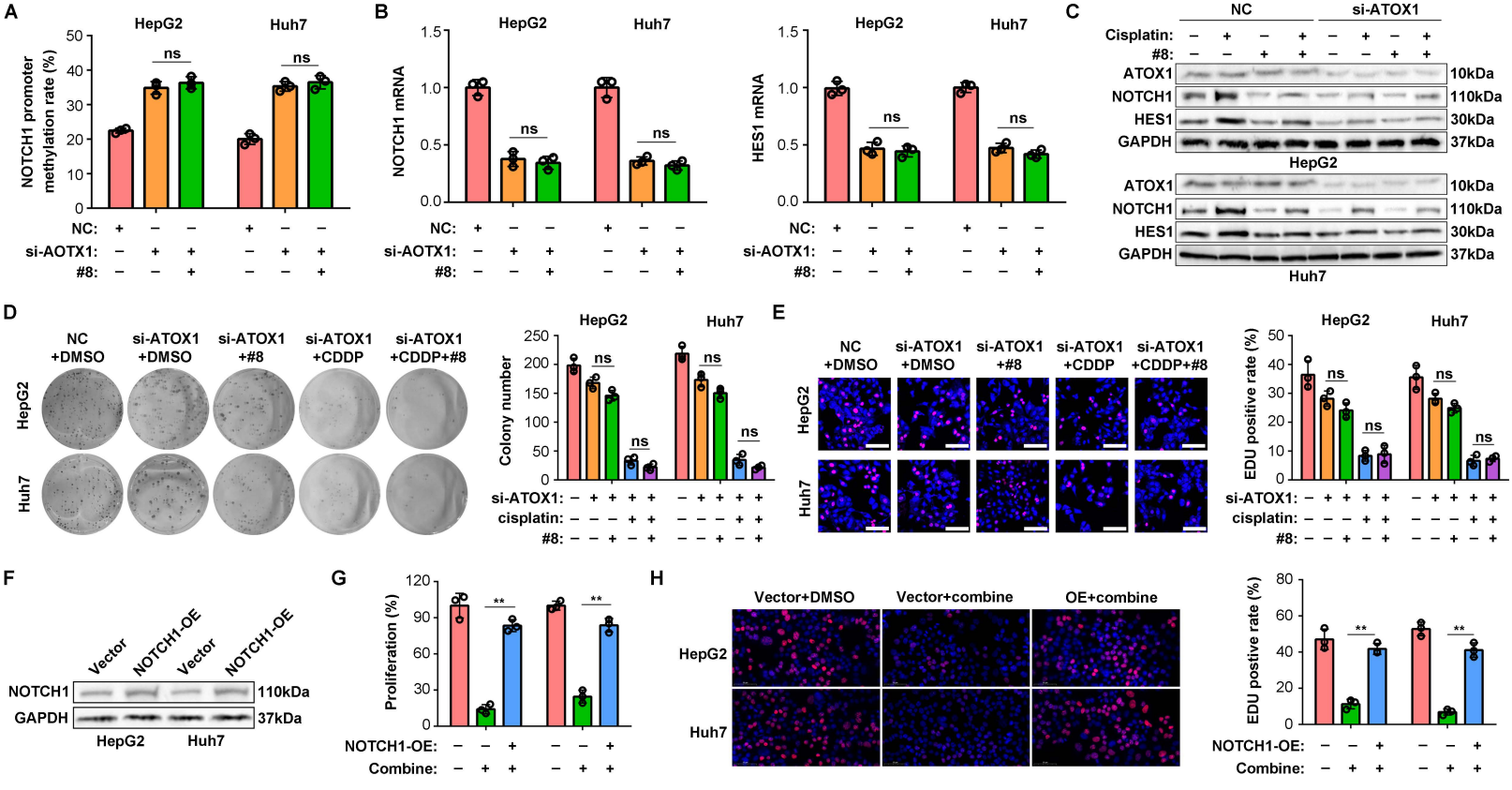
A
HepG2
Huh7
NOTCH1 promoter methylation rate (%)
ns
NC:
si-AOTX1:
#8:
B
HepG2
Huh7
NOTCH1 mRNA
HES1 mRNA
ns
NC:
si-AOTX1:
#8:
C
NC
si-ATOX1
Cisplatin:
#8:
ATOX1
NOTCH1
HES1
GAPDH
10kDa
110kDa
30kDa
37kDa
HepG2
Huh7
D
NC +DMSO
si-ATOX1 +DMSO
si-ATOX1 +#8
si-ATOX1 +CDDP
si-ATOX1 +CDDP+#8
HepG2
Huh7
Colony number
si-ATOX1:
cisplatin:
#8:
E
EDU positive rate (%)
F
Vector
NOTCH1-OE
NOTCH1
GAPDH
110kDa
37kDa
G
Proliferation (%)
NOTCH1-OE:
Combine:
H
Vector+DMSO
Vector+combine
OE+combine
EDU postive rate (%)